A Signal Processing Framework for Agile RF Beamforming: From RF-Chain-Free to Hybrid Beamformers

Sohail Payami, *Member, IEEE*, Konstantinos Nikitopoulos, *Senior Member, IEEE*, Mohsen Khalily, *Senior Member, IEEE*, and Rahim Tafazolli, *Senior Member, IEEE*

***Abstract*— In conventional hybrid beamforming approaches, the number of radio-frequency (RF) chains is the bottleneck on the achievable spatial multiplexing gain. Recent studies have overcome this limitation by increasing the update-rate of the RF beamformer. This paper presents a framework to design and evaluate such approaches, which we refer to as *agile RF beamforming*, from theoretical and practical points of view. In this context, we consider the impact of the number of RF-chains, phase shifters' speed, and resolution to design agile RF beamformers. Our analysis and simulations indicate that even an RF-chain-free transmitter, which its beamformer has no RF-chains, can provide a promising performance compared with fully-digital systems and significantly outperform the conventional hybrid beamformers. Then, we show that the phase shifter's limited switching speed can result in signal aliasing, in-band distortion, and out-of-band emissions. We introduce performance metrics and approaches to measure such effects and compare the performance of the proposed agile beamformers using the Gram-Schmidt orthogonalization process. Although this paper aims to present a generic framework for deploying agile RF beamformers, it also presents extensive performance evaluations in communication systems in terms of adjacent channel leakage ratio, sum-rate, power efficiency, error vector magnitude, and bit-error rates.**

***Index Terms*— Agile RF beamforming, RF-chain-free beamforming, analog beamforming, hybrid beamforming.**

I. Introduction

FULLY-DIGITAL beamformers, with a dedicated radio-frequency (RF) chain per antenna, provide a high level of flexibility and accuracy to control the amplitude and phase of the signal at each antenna element in multiple-input multiple-output (MIMO) systems. Theoretical studies [1], [2] and practical trials [3]–[7] show that massive MIMO systems, where the base station is equipped with a large number of antennas, can provide significant performance gains both in sub-6 GHz [3] and millimeter wave (mmWave) systems [4]–[7]. Deploying digital beamformers, however, increases the cost and power consumption of MIMO technologies. Hence, analog and hybrid beamformers have recently gained significant interest as an alternative approach to digital beamformers, particularly for systems with a large number of antennas [2], [8], [9]. Hybrid beamformers can be used in both sub-6 GHz [8], [10], [11] and mmWave frequencies [12]. MmWave systems, generally, need a larger number of antennas and the cost and complexity of digital beamformers for such systems is relatively higher than sub-6 GHz technologies. Hence, hybrid beamformers have attracted more attention in the context of mmWave applications. For example, [12] leverages the sparse nature of mmWave systems to design the hybrid beamforming weights of a fully-connected structure. The authors in [13] propose a successive interference cancellation based hybrid precoding for subconnected architectures. Based on the angular properties of mmWave channels, [14] proposes codebook based approaches for fully-connected and subconnected hybrid beamformers in a single-user scenario where the quantization bits are nonuniformly assigned to different coverage angles. The authors in [15] treat the hybrid beamforming problem for mmWave systems as a matrix factorization problem and employ alternating minimization algorithms to propose low-complexity solutions. In the context of internet of things (IoT) applications in mmWave scenarios, [16] proposes a low-complexity hybrid precoding and diversity combining by grouping the spatial subchannels of mmWave channel into several lobes. Considering a wideband multiuser scenario, [17] exploits the angle-of-arrival properties and covariance matrix of mmWave to calculate the beamforming weights.

Analog/hybrid beamformers, generally, consist of a phase shifter network that connects one/several RF-chain(s) to a larger number of antennas. In conventional analog and hybrid beamforming approaches, the phase shifters of the RF beamformer retain their phase during the channel's coherence time [2], [8]–[11]. In such systems, however, the number of RF-chains is the upper-bound on the achievable spatial multiplexing gain [18]. Hence, even if the propagation channel allows for the transmission of a larger number of concurrently transmitted data streams, conventional approaches may not be able to fully exploit the

Manuscript received July 19, 2020; revised December 22, 2020; accepted February 12, 2021. Date of publication February 22, 2021; date of current version June 16, 2021. The associate editor coordinating the review of this article and approving it for publication was S. Affe. *(Corresponding author: Sohail Payami.)*

The authors are with the 5G and 6G Innovation Centres, Institute for Communication Systems (ICS), University of Surrey, Guildford GU2 7XH, U.K. (e-mail: sohail.payami@surrey.ac.uk; k.nikitopoulos@surrey.ac.uk; m.khalily@surrey.ac.uk; r.tafazolli@surrey.ac.uk).

Color versions of one or more figures in this article are available at https://doi.org/10.1109/TCOMM.2021.3061101.

Digital Object Identifier 10.1109/TCOMM.2021.3061101

potential of MIMO channels to provide higher data rates and connectivity.

Recently, there have been several attempts, as in [19]–[23] and references therein, towards achieving a higher order of spatial multiplexing gain than the number of the RF-chains using different transmitter structures. For example, electronically steerable parasitic array radiation (ESPAR) antennas and load modulated MIMO can fulfil this target by rapidly changing the loads' impedance [19], [20]. However, one of the disadvantages of such approaches is that the array size needs to be either very small or very large [19], [20]. To overcome some of the limitations of ESPAR and load modulated MIMO, outphasing MIMO uses a tree-structured phase shifter network in conjunction with hybrid couplers [20]. However, scaling up the number of the antennas results in a dramatic increase in the number of the required phase shifters. Consequently, the hardware complexity and computational overhead of the beamformer significantly increase with the array size and the phase shifters' resolution. Assuming that the receiver samples the signal at Nyquist rate and there is perfect synchronization between the sampling time of the transmitter and receiver, [21]–[23] show that analog and hybrid beamformers, with simpler structures compared to [20], can nearly achieve the performance of a fully-digital beamformer.

In short, the spatial multiplexing gain by conventional approaches, such as [2], [8]–[11], [18], is upper-bounded by the number of RF-chains whereas this limit can be overcome by [19]–[23]. The key difference between the approach of [2], [8]–[11], [18] and [19]–[23] is the update-rate of the RF components. To distinguish the two beamforming strategies, we categorize them into conventional and *agile beamformers*. In conventional analog and hybrid beamforming, the elements of the RF beamformer are updated according to the channel's coherence time. On the other hand, we refer to the second approach as agile RF beamforming since it requires the RF beamformer to be agile in updating its weights at a much higher rate than the conventional approaches. However, each time that the phases of the phase shifters are updated, the transmit signal can experience sudden changes and distortion compared to the desired signal generated by a digital transmitter. As we will discuss in detail, this can translate into power leakage to undesired frequency components, interference on adjacent frequency bands, aliasing and in-band signal loss and distortion.

To our knowledge, the existing literature on agile RF beamformers does not provide a comprehensive view of design considerations, approaches, and consequences of using such systems. This paper presents a framework to design and evaluate agile RF beamformers from both theoretical and practical points of view. Within this context, we propose several methods and use simulations to investigate the impact of the number of RF-chains, phase shifters' speed and resolution, signal's bandwidth on the system performance. Starting with a theoretical scenario, we show that an arbitrary signal can be created at the transmitter antennas, without a need for even a single RF-chain, if the phase shifters' resolution and speed are infinitely high. In particular, an RF-chain-free system with two infinitely fast analog phase shifters (APS) per antenna and a carrier signal generator can produce any transmit signal. In practice, most of the phase shifters are digital, and many transmitters may have one or several RF-chains. Compared with APS, the use of digital phase shifters (DPS) can increase the beamformer's computational complexity and can degrade the performance of the analog/hybrid beamformer. On the other hand, using more RF chains can improve performance at the cost of increasing the system cost, complexity, and power consumption. With this motivation, first, we propose low-complexity, while effective, agile RF beamforming methods for the RF-chain-free, analog, and hybrid beamformers with infinitely fast APS, and also DPS. Considering that the phase shifters, in a physical world, have a finite speed, we also propose agile RF beamforming techniques tailored to RF-chain-free, analog, and hybrid beamformers with finite-speed APS and DPS. Then, we analyze the consequences of the phase shifters' switching time on the spectrum of the transmit signal by agile RF-chain-free beamformers. We show that the signal can experience aliasing, in-band loss and distortion, and cause out-of-band-emissions depending on the phase shifters' switching speed and the properties of the transmit signal. Then, we propose agile analog and hybrid beamforming methods that can reduce/alleviate the undesired effects caused by the limited switching speed of the phase shifters. To quantify the undesired effects and compare the performance of different methods towards creating an arbitrarily-designed wireless signal, we propose several performance metrics using the Gram-Schmidt orthogonalization process and normalized mean squared error (MSE). The advantage of such metrics lies in the fact that they solely provide a comparison between two signals in an abstract space, regardless of the intrinsic properties of the reference signal. Using computer simulations, we investigate the impact of system design parameters, such as the resolution and speed of the phase shifters, signal bandwidth, the number of the RF-chains, and antennas on the performance. Finally, in order to provide insights into the expected behavior of the agile RF beamformers in communication systems, we also present extensive simulations for evaluating the impact of the switching-time of the phase shifters on the adjacent channel leakage ratio (ACLR), achievable sum-rates, power efficiency, root mean squared (RMS) error vector magnitude of the received signal based on quadrature amplitude modulation (QAM) constellation, and bit error rates (BER).

This paper is organized as follows: Section II presents the system model, and a brief overview of the conventional beamforming approaches. Section III discusses the principles of agile RF beamforming and proposes design approaches based on the transmitter' s constraints. In particular, subsections III-A and III-B focus on agile RF-chain-free beamformers with infinitely fast APS and DPS, respectively. Subsections III-C and III-D propose agile RF beamforming methods for analog and hybrid beamformers with infinitely fast phase shifters. Subsections III-E, III-F and III-G present the implications of phase shifters' finite switching speed on the performance of agile RF-chain-free, analog and hybrid beamformers, respectively. Section IV introduces performance metrics and presents simulation results to evaluate the performance

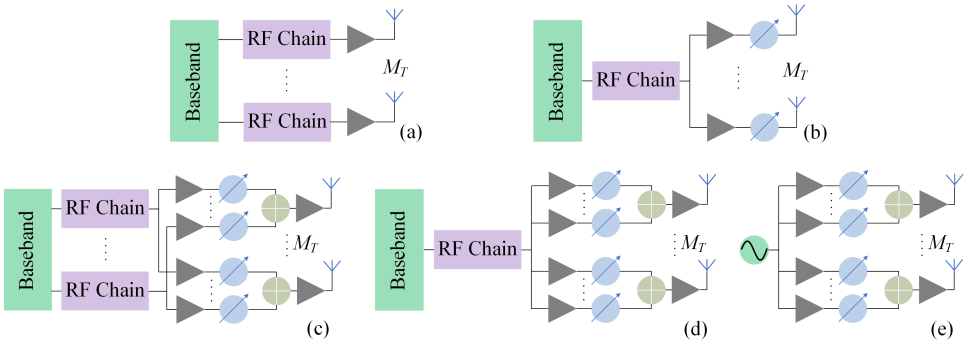

Fig. 1. Block diagram of (a) fully-digital, (b) conventional analog, (c) fully-connected hybrid, d) proposed analog, and e) RF-chain-free beamformers.

of the proposed approaches. Finally, section V discusses the conclusions and the future directions of this research.

Notations: The following notation is used throughout this paper: $\mathbb{R}$ and $\mathbb{C}$ are the field of real and complex numbers. $a(t)$ and $\tilde{a}(f)$ present a variable in the time and frequency domains, receptively. $\mathbf{A}$ and $\mathbf{a}$ represent a matrix and vector. b_n denotes the n-th element of vector $\mathbf{b}$, and $\mathbf{a}_m$ is the m-th column of $\mathbf{A}$. Moreover, $A_{m,n}$, $|A_{m,n}|$, $\angle A_{m,n}$ denote the (m,n)-th element of $\mathbf{A}$, its magnitude and phase, respectively. $\mathbf{A}^{\dagger}$ and $\mathbf{A}^{\mathrm{H}}$ present pseudo-inverse and Hermitian of $\mathbf{A}$. $\mathcal{CN}(\mathbf{a},\mathbf{A})$ presents a random vector of complex Gaussian distributed elements with expected value $\mathbf{a}$ and covariance matrix $\mathbf{A}$. Finally, $\mathrm{E}_{X,Y}[a]$ denotes the expected value of a with respect to variables X and Y.

II. System Model and Conventional Beamforming

Consider a multiantenna transmitter with M_{T} antennas that transmits a signal to $M_{\mathrm{R}} < M_{\mathrm{T}}$ receiver antennas. For the sake of clarity, we use the following terminology in the rest of this paper: the baseband and low-pass signals refer to the discrete-time signal in the processor and the corresponding continuous-time signal at the output of digital-to-analog converter (DAC), respectively. The band-pass signal at the transmitter antennas refers to the continuous-time signal in the RF domain, i.e., after upconverting the low-pass signal. An RF-chain refers to a series of electrical components, e.g., DAC, mixer and local oscillator, that are used to convert the baseband signal into a band-pass signal.

Depending on the number of the RF-chains C, as shown in Fig. 1(a)-Fig. 1(e), the beamformers can be categorized as fully-digital, analog, hybrid and RF-chain-free where $C = M_{\mathrm{T}}$, $C = 1$, $1 < C < M_{\mathrm{T}}$ and $C = 0$, respectively. Moreover, each of these beamformers can be further divided based on the structure of their phase shifter network. For example, Fig. 1(b) and Fig. 1(d) show two realizations of analog beamformers with a single RF-chain. We further divide the beamforming techniques into conventional and agile approaches. If the phase shifters switch their phase according to the coherence time of the channel, then the beamformer is based on a conventional approach. On the hand, if the phase shifters switch their phase faster than the coherence time of the channel, then the corresponding beamformer is based on agile RF beamforming. The subscript $u \in \{\mathrm{D}, \mathrm{CH}, \mathrm{AH}, \mathrm{AA}, \mathrm{ARF}\}$ is used throughout the paper to differentiate the notation for each of the structures and methods. In particular, D, CH, AH, AA, ARF present the notation for digital, conventional hybrid, agile hybrid, agile analog, agile RF-chain-free beamformers, respectively. Table I presents a summary of the notations and symbols that are commonly used throughout the paper.

The low-pass transmit signal vector is denoted by $\mathbf{x}_u(t) \in \mathbb{C}^{M_{\mathrm{T}}\times 1}$ and $\tilde{\mathbf{x}}_u(f) \in \mathbb{C}^{M_{\mathrm{T}}\times 1}$ in the time t and frequency f domains, respectively. In the following, the dependency on time (t) and frequency (f) may be occasionally withdrawn where it can be inferred from the context. Similarly, $\mathbf{y}_u(t) \in \mathbb{C}^{M_{\mathrm{R}}\times 1}$, $\mathbf{z}(t) \in \mathbb{C}^{M_{\mathrm{R}}\times 1}$, $\mathbf{H}(t) \in \mathbb{C}^{M_{\mathrm{R}}\times M_{\mathrm{T}}}$, $\tilde{\mathbf{y}}_u(f) \in \mathbb{C}^{M_{\mathrm{R}}\times 1}$, $\tilde{\mathbf{z}}(f) \in \mathbb{C}^{M_{\mathrm{R}}\times 1}$ and $\tilde{\mathbf{H}}(f) \in \mathbb{C}^{M_{\mathrm{R}}\times M_{\mathrm{T}}}$ denote the received signal and noise vectors and the channel matrix in the time and frequency domains, respectively. A general relationship between the low-pass transmitted and received signals is

$$\tilde{\mathbf{y}}_u(f) = \tilde{\mathbf{H}}(f)\ \tilde{\mathbf{x}}_u(f)\ + \tilde{\mathbf{z}}(f), \tag{1}$$

The continuous-time band-pass signal at the antennas is modelled by $\mathbf{x}_{\mathrm{u}}^{\mathrm{Ant.}}(t) = \cos(2\pi f_{\mathrm{c}} t)\mathbf{x}_{\mathrm{u}}(t)$, where f_{c} denotes the carrier frequency. The following subsections briefly review the process of generating baseband signals by fully-digital and conventional hybrid beamformers.

A. Digital Beamformers

The availability of an RF-chain per antenna, as shown in Fig. 1(a), allows the digital beamformer to, almost continuously, control the phase and amplitude of elements of $\mathbf{x}_{\mathrm{D}}(t)$. Without loss of generality, in the following we only discuss linear beamforming in a multicuarrier system with a total number of K subcarriers. The bandwidth of the transmit signal is $B = \tilde{K}\Delta f$ where $\tilde{K}$ and Δf denote the number of non-zero subcarriers and the subcarrier spacing, respectively. Assuming that $\tilde{K}$ is an even number, the non-zero subcarriers are occupied by zero-mean Gaussian entry inputs $\tilde{\mathbf{s}}(k) \in \mathbb{C}^{M_{\mathrm{U}}\times 1}$, $-\tilde{K}/2 \le k \le \tilde{K}/2$ and $k \neq 0$ where M_{U} is the number of simultaneously transmit streams. In linear beamforming, the transmitter applies the precoding matrix $\tilde{\mathbf{F}}_{\mathrm{D}}(k) \in \mathbb{C}^{M_{\mathrm{T}}\times M_{\mathrm{U}}}$ and the baseband signal vector is $\tilde{\mathbf{x}}_{\mathrm{D}}^{\mathrm{Base.}}(k) = \gamma_{\mathrm{D}}(k)\tilde{\mathbf{F}}_{\mathrm{D}}(k)\tilde{\mathbf{s}}(k)$, where $\gamma_{\mathrm{D}}(k)$ is a power normalization factor. The spatial multiplexing gain in digital beamformers is upper-bounded by the rank of $\tilde{\mathbf{H}}(k)$, which can be up to $\min(M_{\mathrm{T}}, M_{\mathrm{R}})$.

TABLE I
SUMMARY OF THE NOTATION AND DESCRIPTION OF THE VARIABLES THAT ARE COMMONLY USED IN THIS MANUSCRIPT

Notation	Description	Notation	Description
M_{R}	Number of receiver antennas	t	Continuous time
M_{T}	Number of transmitter antennas	n	Discrete time index
'u'	$u \in$ {D, CH, AH, AA, ARF}	f	Continuous frequency
'D'	Digital	k	Subcarrier index
'ARF'	Agile RF-chain-free	f_{c}	Carrier frequency
'AA'	Agile analog	Δf	Subcarrier spacing
'AH'	Agile hybrid	K	Total number of subcarriers
'APS'	Analog phase shifters	$\check{K}$	Number of non-zero subcarriers
'DPS'	Analog phase shifters	M_{U}	Number of transmit streams
B	Bandwidth	T_{SW}	Switching-time of phase shifters
γ_u	Power normalization factor for structure u	Q	Resolution of phase shifters
$\mathbf{H}$	Channel matrix	T_{S}	Sampling time
$\mathbf{z}(t)$	Low-pass time-domain noise vector	C	Number of RF chains
$\mathbf{x}_u^{\text{Ant.}}(t)$	Continuous-time band-pass transmit signal at the antennas of system u	$\mathbf{x}_u(t)$	Continuous-time low-pass transmit signal at the antennas of system u
$\mathbf{y}_u^{\text{Ant.}}(t)$	Continuous-time band-pass received signal from the antennas of system u	$\mathbf{y}_u(t)$	Continuous-time low-pass received signal from the antennas of system u
$\tilde{\mathbf{y}}_u(f)$	Frequency-domain representation of $\mathbf{y}_u(t)$	$\tilde{\mathbf{x}}_u(f)$	Frequency-domain representation of $\mathbf{x}_u(f)$
$\tilde{\mathbf{s}}(k)$	Transmit symbol vector on subcarrier k	$\tilde{\mathbf{x}}_u^{\text{Base.}}(k)$	Baseband transmit signal over subcarrier k in system u

B. Conventional Analog and Hybrid Beamformers

As shown in Fig. 1(b)-Fig. 1(d), the baseband of such systems is connected to M_{T} antennas via C RF-chain(s) and a network of phase shifters. In particular, the case for $C = 1$ and $C \geq 2$ are referred to as analog and hybrid beamformers, respectively. In a conventional hybrid beamformer with a linear digital precoder, the baseband model for the transmit signal is

$$\tilde{\mathbf{x}}_{\mathrm{CH}}^{\text{Base.}}(k) = \gamma_{\mathrm{CH}}(k)\mathbf{F}_{\mathrm{CH}}\tilde{\mathbf{B}}_{\mathrm{CH}}(k)\tilde{\mathbf{s}}(k), \tag{2}$$

where $\gamma_{\mathrm{CH}}(k)$, $\mathbf{F}_{\mathrm{CH}} \in \mathbb{C}^{M_{\mathrm{T}} \times C}$ and $\mathbf{B}_{\mathrm{CH}} \in \mathbb{C}^{C \times M_{\mathrm{R}}}$ are power normalization factor, the RF beamforming and baseband precoding matrices, respectively. The elements of $\mathbf{F}_{\mathrm{CH}}$ with APS are in the form of $F_{\mathrm{CH},m_{\mathrm{T}},c} = e^{j\theta_{m_{\mathrm{T}},c}}$, where $\theta_{m_{\mathrm{T}},c} \in [0, 2\pi)$ and $m_{\mathrm{T}} \in \{1, \ldots, M_{\mathrm{T}}\}$. If the beamformer is equipped with DPS with Q bits of resolution, then $\theta_{m_{\mathrm{T}},c} \in \{0, \ldots, (2^Q - 1)2\pi/2^Q\}$. In conventional analog and hybrid beamforming, the RF beamformer remains constant during the coherence time of the channel. Consequently, the phase shifters provide the same phase shift to all of the subcarriers [10], [24]. This limitation combined with the constant modulus constraint, imposed by phase shifters, makes the design of hybrid beamformers a challenging problem, particularly for frequency-selective channels [17]. Moreover, most of the commercial phase shifters are digitally controlled and have discrete resolution. This, in turn, can significantly increase the computational complexity of designing optimal hybrid beamformers. Another limitation of conventional analog and hybrid beamformers is that the spatial multiplexing gain is limited by the rank of the RF beamforming matrix and the number of RF-chains [2]. In other words, the conventional methods cannot transmit $M_{\mathrm{U}} \geq C$ simultaneous streams, even if the propagation channel allows it. In the next subsection, we show that agile RF beamforming methods and structures that can overcome the limitations of conventional approaches.

III. AGILE RF BEAMFORMING

Agile RF beamformers can achieve a higher order of spatial multiplexing gain than the number of RF-chains. In this work, we only focus on transmitter structures that employ phase shifters, as shown in Fig. 1(b) to Fig. 1(e). Agile RF beamformers can ideally create any transmit signal by a fully-digital beamformer while using a much smaller number of RF-chains. Consequently, they can create signals at the transmitter antennas such that (s.t.) $M_{\mathrm{U}} \geq C$, instead of $M_{\mathrm{U}} \leq C$ by the conventional approaches. Agile RF beamformers leverage the following principle: as long as the received signal vector remains the same as $\mathbf{y}_{\mathrm{D}}^{\text{Ant.}}(t)$ at the user equipment, the receiver operations and system performance will not be affected. Hence, regardless of the transmitter's structure, e.g., Fig. 1(c) or Fig. 1(d), the system's performance remains the same if $\mathbf{y}_{\mathrm{D}}^{\text{Ant.}}(t) = \mathbf{y}_u^{\text{Ant.}}(t)$, or equivalently,

$$\|\mathbf{y}_{\mathrm{D}}^{\text{Ant.}}(t) - \mathbf{y}_{\mathrm{u}}^{\text{Ant.}}(t)\|^2 = 0, \tag{3}$$

$\forall u \in \{\text{AH, AA, ARF}\}$. Equation (3) is equivalent to $\|\mathbf{x}_{\mathrm{D}}^{\text{Ant.}}(t) - \mathbf{x}_u^{\text{Ant.}}(t)\|^2 = 0$, as $\tilde{\mathbf{y}}_u(f) = \tilde{\mathbf{H}}(f)\tilde{\mathbf{x}}_u(f) + \tilde{\mathbf{z}}(f)$. In this direction, we employ minimum mean squared error (MMSE) criteria to design $\mathbf{x}_u^{\text{Ant., opt}}(t)$ by the agile beamformer. In particular,

$$\mathbf{x}_u^{\text{Ant., opt}}(t) = \underset{\mathbf{x}_u^{\text{Ant.}}(t)}{\arg\min} \|\mathbf{x}_{\mathrm{D}}^{\text{Ant.}}(t) - \mathbf{x}_u^{\text{Ant.}}(t)\|^2. \tag{4}$$

Strictly speaking, if $\mathbf{x}_{\mathrm{D}}^{\text{Ant.}}(t)$ can achieve a spatial multiplexing gain of $M_{\mathrm{U}} \geq C$, so does $\mathbf{x}_u^{\text{Ant., opt}}(t)$ if $\|\mathbf{x}_{\mathrm{D}}^{\text{Ant.}}(t) - \mathbf{x}_u^{\text{Ant., opt}}(t)\|^2 = 0$, $\forall t$. To meet this criteria, first, system u must provide the same amplitude and phase value at any given time $t \in (-\infty, +\infty)$ so that $x_{u,m_{\mathrm{T}}}(t) = x_{\mathrm{D},m_{\mathrm{T}}}(t)$. As a result, the conventional analog beamformer shown in Fig. 1(b), with one phase shifter per antenna, cannot fulfill this condition, in a general scenario, since $|x_{\mathrm{D},m_{\mathrm{T}}}(t_0)| \neq |x_{\mathrm{D},m'_{\mathrm{T}}}(t_0)|$ may not hold for all $m_{\mathrm{T}} \neq m'_{\mathrm{T}}$. The second condition to achieve $\|\mathbf{x}_{\mathrm{D}}^{\text{Ant.}}(t) - \mathbf{x}_u^{\text{Ant., opt}}(t)\|^2 = 0$, $\forall t$, is that system u must operate at the same speed as a fully-digital beamformer.

In other words, response time T_{SW} of the phase shifters in Fig. 1(c)-Fig. 1(e) must provide the ability to track $\mathbf{x}_{\text{D}}^{\text{Ant.}}(t)$ in time. For an arbitrary $\mathbf{x}_{\text{D}}^{\text{Ant.}}(t)$, this condition can be only met if $T_{\text{SW}} \to 0$ which requires the phase shifters to be infinitely fast.

In the rest of this section, we evaluate the implications of the number of RF-chains, phase shifters' resolution, and response-time on the MMSE design criteria in (4). More specifically, subsections III-A-III-D propose agile RF beamforming methods for RF-chain-free, analog, and hybrid beamformers with infinitely fast phase shifters, i.e., $T_{\text{SW}} \to 0$. Then, subsections III-E- III-G consider the impact of the response time T_{SW} of the phase shifters on agile beamformers' design and performance.

A. Agile RF-Chain-Free Beamformer With APS & $T_{SW} \to 0$

In this subsection, we present an agile RF beamforming method for the RF-chain-free beamformer shown in Fig. 1(e) with infinitely fast APS. In this system, a carrier signal $\cos(2\pi f_{\text{c}} t)$ is fed to the phase shifter network where each antenna is equipped with two APS and a combiner. Let's define vectors $\mathbf{f}_{\text{t}}(t)$ and $\mathbf{f}_{\text{b}}(t)$ to present the phase shifting effect by the phase shifters on each antenna's top and bottom branches, respectively. The transmit signal vector for the RF-chain-free system can be expressed as $\mathbf{x}_{\text{ARF}}^{\text{Ant.}}(t) = \cos(2\pi f_{\text{c}} t)\mathbf{x}_{\text{ARF}}(t) = \gamma_{\text{ARF}} \cos(2\pi f_{\text{c}} t)\big(\mathbf{f}_{\text{t}}(t) + \mathbf{f}_{\text{b}}(t)\big)/2$, where γ_{ARF} and $1/2$ are normalization factors such that the average transmit power from all antennas over the time is $\text{E}_{m_{\text{T}},t}\big[\|\mathbf{x}_{\text{ARF}}^{\text{Ant.}}(t)\|^2\big] = \text{E}_{m_{\text{T}},t}\big[\|\mathbf{x}_{\text{D}}^{\text{Ant.}}(t)\|^2\big] = P$. The agile RF-chain-free beamformer, with $T_{\text{SW}} \to 0$, can create an arbitrary signal $\mathbf{x}_{\text{D}}^{\text{Ant.}}(t)$, if

$$\mathbf{x}_{\text{D}}^{\text{Ant.}}(t) - \mathbf{x}_{\text{ARF}}^{\text{Ant.}}(t) = \cos(2\pi f_{\text{c}} t)\big(\mathbf{x}_{\text{D}}(t) - \mathbf{x}_{\text{ARF}}(t)\big) = 0. \quad (5)$$

Hence, (4) can be reformulated as

$$\begin{aligned}(\mathbf{f}_{\text{t}}^{\text{opt}}, \mathbf{f}_{\text{b}}^{\text{opt}}) &= \underset{\mathbf{f}_{\text{t}},\mathbf{f}_{\text{b}}}{\arg\min} \|\mathbf{x}_{\text{D}}(t) - \mathbf{x}_{\text{ARF}}(t)\|^2 \\ &= \underset{\mathbf{f}_{\text{t}},\mathbf{f}_{\text{b}}}{\arg\min} \left\|\mathbf{x}_{\text{D}}(t)/\gamma_{\text{ARF}} - \frac{\mathbf{f}_{\text{t}}(t) + \mathbf{f}_{\text{b}}(t)}{2}\right\|^2 \\ &= \underset{\mathbf{f}_{\text{t}},\mathbf{f}_{\text{b}}}{\arg\min} \sum_{m_{\text{T}}=1}^{M_{\text{T}}} \left| x_{\text{D},m_{\text{T}}}/\gamma_{\text{ARF}} - \frac{f_{\text{t},m_{\text{T}}} + f_{\text{b},m_{\text{T}}}}{2}\right|^2, \\ &\quad \text{s.t. } \theta_{\text{t},m_{\text{T}}}, \theta_{\text{b},m_{\text{T}}} \in [0, 2\pi). \end{aligned} \quad (6)$$

Previously, [8], [11] have shown that if variable $x \in \{X | X \in \mathbb{C}, |X| \leq 1\}$, then $\exists\ \phi_1, \phi_2 \in [0, 2\pi)$ such that $x = (e^{j\phi_1} + e^{j\phi_1})/2$. Let's define $\bar{\mathbf{x}}_{\text{D}} = \mathbf{x}_{\text{D}}(t)/\gamma_{\text{ARF}}$. Assuming that $|\bar{x}_{\text{D},m_{\text{T}}}(t)| \leq 1$, $m_{\text{T}} \in \{1, 2, \ldots, M_{\text{T}}\}$, then $\exists f_{\text{t},m_{\text{T}}}(t)$, $f_{\text{b},m_{\text{T}}}(t)$ such that

$$\left| \bar{x}_{\text{D},m_{\text{T}}} - \frac{f_{\text{t},m_{\text{T}}}(t) + f_{\text{b},m_{\text{T}}}(t)}{2}\right|^2 = 0. \quad (7)$$

Based on [11], the equality can be achieved by setting $f_{\text{t},m_{\text{T}}}(t)$ and $f_{\text{b},m_{\text{T}}}(t)$ according to

$$\begin{cases} f_{\text{t},m_{\text{T}}}^{\text{opt}}(t) = \text{e}^{j\angle \bar{x}_{\text{D},m_{\text{T}}} + j\cos^{-1}(|\bar{x}_{\text{D},m_{\text{T}}}|)}, \\ f_{\text{b},m_{\text{T}}}^{\text{opt}}(t) = \text{e}^{j\angle \bar{x}_{\text{D},m_{\text{T}}} - j\cos^{-1}(|\bar{x}_{\text{D},m_{\text{T}}}|)}. \end{cases} \quad (8)$$

In order for $|\bar{x}_{\text{D},m_{\text{T}}}(t)| \leq 1$, $\forall\ m_{\text{T}} \in \{1, 2, \ldots, M_{\text{T}}\}$, to hold, the amplitude of the carrier signal must be set such that $\gamma_{\text{ARF}} \geq \max_{t,m_{\text{T}}}\big(|x_{\text{D},m_{\text{T}}}(t)|\big)$.

It should be noted that a similar approach to (8) was previously used to design conventional hybrid beamformers with $C = 2M_{\text{U}}$ [8], [11], and agile RF beamformer with a small number of RF-chain [21], [22]. The approach of [8], [11] underutilizes the achievable spatial multiplexing gain that the propagation channel can provide.

On the other hand, [21], [22] show that a single RF-chain, i.e., $C = 1$ is enough to achieve a higher order of spatial multiplexing gain by considering APS. Despite some similarities between the proposed beamformer of (8) and [8], [11], [20]–[22], in this subsection we showed that, in theory, there is no need for even one RF-chain or even a local oscillator to create an arbitrary transmit signal. In this case, $\mathbf{x}_{\text{D}}^{\text{Ant.}}(t) = \mathbf{x}_{\text{ARF}}^{\text{Ant.}}(t)$ can be achieved for the bandpass signals as long as the phase shifters in in Fig. 1(e) have continuous resolution and $T_{\text{SW}} \to 0$, and the baseband can control the corresponding components at a similar rate. As it will become more clear in the following sections that we impose more realistic constraints on the phase shifters, using a local oscillator as in Fig. 1(e) significantly reduces the stringent requirements for controlling and updating the phase shifters to comply with Nyquist sampling theorem. More specifically, we will show that T_{SW} limits the bandwidth B of the transmit signal in RF-chain-free systems in a similar manner that DACs limit B in digital transmitters. In both cases, using a local oscillator allows the baseband processor to operate at a speed that is related to B instead of the highest frequency of the signal, i.e., $f_{\text{c}} + B/2$. With this background, in the following, we design the agile RF beamformers based for the low-pass models, i.e., $\|\mathbf{x}_{\text{D}}(t) - \mathbf{x}_{\text{ARF}}(t)\|^2$ instead of solving the optimization problem for the equivalent bandpass signals.

In this subsection, we showed that a carrier signal generator and two fast APS per antenna, as shown in Fig. 1(e), are enough to generate $\bar{x}_{\text{D},m_{\text{T}}}(t)$. Hence, if $\mathbf{x}_{\text{D}}(t)$ can support any order of spatial multiplexing gain, so will $\mathbf{x}_{\text{ARF}}(t)$. Next, we consider the impact of using DPS with Q bits of resolutions in such systems.

B. Agile RF-Chain-Free Beamformer With DPS & $T_{SW} \to 0$

This subsection presents an agile RF beamforming approach for the RF-chain-free beamformer shown in Fig. 1(e) with Q-bits resolution DPS assuming $T_{\text{SW}} \to 0$. Similar to subsection III-A, the transmit signal can be decomposed as $\mathbf{x}_{\text{ARF}} = \gamma_{\text{ARF}}(\mathbf{f}_{\text{t}} + \mathbf{f}_{\text{b}})/2$ where $\gamma_{\text{ARF}} \geq \max_{t,m_{\text{T}}}\big(|x_{\text{D},m_{\text{T}}}(t)|\big)$. Let $\mathbf{f}_{\text{t}}^{\text{DPS}}$, $\mathbf{f}_{\text{b}}^{\text{DPS}}$ denote the optimal beamforming weights for the digital phase shifters on the top and bottom branches connected to each antenna, where

$$\begin{aligned}(\mathbf{f}_{\text{t}}^{\text{DPS}}, \mathbf{f}_{\text{b}}^{\text{DPS}}) = \underset{\mathbf{f}_{\text{t}},\mathbf{f}_{\text{b}}}{\arg\min} \|\mathbf{x}_{\text{D}}(t) - \mathbf{x}_{\text{ARF}}(t)\|^2, \\ \text{s.t. } \theta_{\text{t},m_{\text{T}}}, \theta_{\text{b},m_{\text{T}}} \in \{0, \ldots, (2^Q - 1)2\pi/2^Q\}. \end{aligned} \quad (9)$$

Finding the global optimum to this combinatorial and non-convex optimization, in general, is computationally expensive.

In the following, we present a low-complexity sub-optimal approach by sequentially designing $\mathbf{f}_{\mathrm{t}}^{\mathrm{DPS}}$ and $\mathbf{f}_{\mathrm{b}}^{\mathrm{DPS}}$. Given that $\mathbf{f}_{\mathrm{t}}^{\mathrm{opt}}$ of (8) is an optimal solution when APS are used, we calculate the beamforming weights $\mathbf{f}_{\mathrm{t}}^{\mathrm{DPS}}$ for DPS according to

$$\begin{aligned}\mathbf{f}_{\mathrm{t}}^{\mathrm{DPS}} &= \arg\min_{\mathbf{f}_{\mathrm{t}}} \|\mathbf{f}_{\mathrm{t}}^{\mathrm{opt}} - \mathbf{f}_{\mathrm{t}}\|^2 \\ &= \arg\min_{f_{\mathrm{t},m_{\mathrm{T}}}} \sum_{m_{\mathrm{T}}=1}^{M_{\mathrm{T}}} |f_{\mathrm{t},m_{\mathrm{T}}}^{\mathrm{opt}} - f_{\mathrm{t},m_{\mathrm{T}}}|^2, \\ &= \sum_{m_{\mathrm{T}}=1}^{M_{\mathrm{T}}} \arg\min_{f_{\mathrm{t},m_{\mathrm{T}}}} |f_{\mathrm{t},m_{\mathrm{T}}}^{\mathrm{opt}} - f_{\mathrm{t},m_{\mathrm{T}}}|^2, \\ &\quad \text{s.t. } \theta_{\mathrm{t},m_{\mathrm{T}}} \in \{0, \ldots, (2^Q-1)2\pi/2^Q\}. \end{aligned} \tag{10}$$

It can be easily verified that this is equivalent to

$$\begin{aligned}\angle f_{\mathrm{t},m_{\mathrm{T}}}^{\mathrm{DPS}}(t) &= \mathcal{Q}\big(f_{\mathrm{t},m_{\mathrm{T}}}^{\mathrm{opt}}(t)\big) \\ &= \arg\min_{\angle f_{\mathrm{t},m_{\mathrm{T}}}(t)} |\angle f_{\mathrm{t},m_{\mathrm{T}}}^{\mathrm{opt}}(t) - \angle f_{\mathrm{t},m_{\mathrm{T}}}(t)|^2, \\ &\quad \text{s.t. } \theta_{\mathrm{t},m_{\mathrm{T}}}(t) \in \{0, \ldots, (2^Q-1)2\pi/2^Q\}. \end{aligned} \tag{11}$$

The quantizer function $\mathcal{Q}\big(f_{\mathrm{t},m_{\mathrm{T}}}^{\mathrm{opt}}\big)$ rounds the phase of $f_{\mathrm{t},m_{\mathrm{T}}}^{\mathrm{opt}}$ to the closest discrete phase value available to the corresponding phase shifter. By inserting $\mathbf{x}_{\mathrm{ARF}} = \gamma_{\mathrm{ARF}}(\mathbf{f}_{\mathrm{t}}^{\mathrm{DPS}} + \mathbf{f}_{\mathrm{b}})/2$ in (9),

$$\begin{aligned}\mathbf{f}_{\mathrm{b}}^{\mathrm{DPS}} &= \arg\min_{\mathbf{f}_{\mathrm{b}}} \|\mathbf{x}_{\mathrm{D}}(t) - \mathbf{x}_{\mathrm{ARF}}(t)\|^2 \\ &= \arg\min_{\mathbf{f}_{\mathrm{b}}} \Big\|\mathbf{x}_{\mathrm{D}}/\gamma_{\mathrm{ARF}} - \frac{\mathbf{f}_{\mathrm{t}}^{\mathrm{DPS}}}{2} - \frac{\mathbf{f}_{\mathrm{b}}}{2}\Big\|^2 \\ &= \sum_{m_{\mathrm{T}}=1}^{M_{\mathrm{T}}} \arg\min_{f_{\mathrm{b},m_{\mathrm{T}}}} \Big|w_{m_{\mathrm{T}}} - \frac{f_{\mathrm{b},m_{\mathrm{T}}}}{2}\Big|^2, \\ &\quad \text{s.t. } \theta \in \{0, \ldots, (2^Q-1)2\pi/2^Q\}. \end{aligned} \tag{12}$$

where $\mathbf{w} = \mathbf{x}_{\mathrm{D}}/\gamma_{\mathrm{ARF}} - \mathbf{f}_{\mathrm{t}}^{\mathrm{DPS}}/2$. Based on (10) and (11), it can be easily verified that

$$\angle f_{\mathrm{b},m_{\mathrm{T}}}^{\mathrm{DPS}}(t) = \mathcal{Q}\big(w_{m_{\mathrm{T}}}(t)\big). \tag{13}$$

In this subsection, we presented a low-complexity agile RF-chain-free beamforming approach for the structure of Fig. 1(e) with DPS. As it will show by simulations, the proposed method results in a promising performance if $Q \geq 5$. Next, we explore the consequences of using an RF-chain by an analog beamformer, compared to the RF-chain-free systems.

C. Agile Analog Beamformer With $T_{SW} \to 0$

This subsection presents an agile RF beamforming approach for the analog beamformer shown in Fig. 1(d) assuming $T_{\mathrm{SW}} \to 0$. In the proposed RF-chain-free approach, regardless of the angular resolution of the phase shifters, the amplitude of the input signal to the phase shifter network depends on $\max_{t,m_{\mathrm{T}}}\big(|x_{\mathrm{D},m_{\mathrm{T}}}(t)|\big)$. In other words, the input power to the phase shifter network is related to the highest power from all antennas $m_{\mathrm{T}} \in \{1, 2, \ldots, M_{\mathrm{T}}\}$ over all times $t \in (-\infty, +\infty)$. Given that the feed network equally distributes the power among all phase shifters, the extra input power to the elements on the m_{T}-th antenna must be dissipated at the corresponding combiner when $|x_{\mathrm{D},m_{\mathrm{T}}}(t)| < \max_{t,m_{\mathrm{T}}}\big(|x_{\mathrm{D},m_{\mathrm{T}}}(t)|\big)$. This, in turn, can significantly increase the dynamic losses and reduce the energy efficiency of the system depending on the characteristics and fluctuations of the transmit signal. When an RF-chain is available, the baseband and DAC can swiftly control the input power to the phase shifter network at any given time t. As a result, the amplitude of the input signal to the phase shifters and, consequently, the dissipated power at the combiner, are related to $\max_{m_{\mathrm{T}}}\big(|x_{\mathrm{D},m_{\mathrm{T}}}(t)|\big)$, unlike $\max_{t,m_{\mathrm{T}}}\big(|x_{\mathrm{D},m_{\mathrm{T}}}(t)|\big)$ for the RF-chain-free system. An RF-chain also provides an additional degrees of freedom to control both the phase and magnitude of the input signal to the phase shifter network, and it can be also used to further reduce the MSE

$$\begin{aligned}&\|\mathbf{x}_{\mathrm{D}}(t) - \mathbf{x}_{\mathrm{AA}}(t)(t)\|^2 \\ &\quad = \|\mathbf{x}_{\mathrm{D}}(t)\|^2 + \|\mathbf{x}_{\mathrm{AA}}(t)\|^2 - 2\mathrm{real}(\mathbf{x}_{\mathrm{D}}^{\mathrm{H}}(t)\mathbf{x}_{\mathrm{AA}}(t)), \\ &\qquad \text{s.t. } \theta_{\mathrm{t},m_{\mathrm{T}}}(t), \theta_{\mathrm{b},m_{\mathrm{T}}}(t) \in \{0, \ldots, (2^Q-1)2\pi/2^Q\}, \end{aligned} \tag{14}$$

compared to an RF-chain-free system. The transmit signal vector by the agile analog beamformer can be written as

$$\mathbf{x}_{\mathrm{AA}}(t) = b(t)\mathbf{f}(t) = b(t)(\mathbf{f}_{\mathrm{t}} + \mathbf{f}_{\mathrm{b}})/2 \tag{15}$$

where $\mathbf{f}(t) = (\mathbf{f}_{\mathrm{t}} + \mathbf{f}_{\mathrm{b}})/2$, and $b(t)$ is a scalar complex number at the output of DAC. To design $\mathbf{x}_{\mathrm{AA}}(t)$ that minimizes MSE, considering the nonconvex constraints of $\mathbf{f}_{\mathrm{t}}$ and $\mathbf{f}_{\mathrm{b}}$, let's decouple the optimization of the baseband signal and the phases of the phase shifters. Setting $\mathbf{f}_{\mathrm{t}}^{\mathrm{DPS}}$ and $\mathbf{f}_{\mathrm{b}}^{\mathrm{DPS}}$ according to equations (11) and (13), as for the RF-chain-free system, the optimal baseband weight $b^{\mathrm{opt}}(t)$ becomes

$$b^{\mathrm{opt}}(t) = \arg\min_{b(t)} \|\mathbf{f}^{\mathrm{DPS}}\|^2|b|^2 - 2\mathrm{real}(\mathbf{x}_{\mathrm{D}}^{\mathrm{H}}\mathbf{f}^{\mathrm{DPS}}e^{j\angle b})|b| + \|\mathbf{x}_{\mathrm{D}}\|^2. \tag{16}$$

It can be easily verified that the second-order function in (16) is minimized if

$$\begin{cases} |b^{\mathrm{opt}}(t)| = \big|\mathbf{x}_{\mathrm{D}}^{\mathrm{H}}(t)\mathbf{f}^{\mathrm{DPS}}(t)\big|/\|\mathbf{f}^{\mathrm{DPS}}(t)\|^2, \\ \angle b^{\mathrm{opt}}(t) = -\angle(\mathbf{x}_{\mathrm{D}}^{\mathrm{H}}(t)\mathbf{f}^{\mathrm{DPS}}(t)). \end{cases} \tag{17}$$

In this subsection, we discussed that the RF-chain of the analog beamformer can reduce the dissipated power at the combiners before the antennas, compared to RF-chain-free systems. We also presented a low-complexity approach for designing agile analog beamformers with DPS. The RF-chain in the system provides a degree of freedom to reduce the MSE compared to RF-chain-free systems. Our simulations in section IV show that using an RF-chain can reduce the MSE when the number of antennas are relatively small. However, as M_{T} increases, the MSE increases until it reaches a saturation level. In other words, one RF-chain may not be always sufficient to substantially reduce the MSE for large arrays. Next, we generalize the proposed approaches to hybrid beamforming structures with several RF-chains.

D. Agile Hybrid Beamformer With $T_{SW} \to 0$

This subsection presents an agile RF beamforming approach for the fully-connected hybrid beamformer with C RF-chains

shown in Fig. 1(c) assuming $T_{\text{SW}} \rightarrow 0$. The transmit signal vector for this structure is $\mathbf{x}_{\text{AH}}(t) = \mathbf{F}(t)\mathbf{b}(t)$ where $\mathbf{F}(t) \in \mathbb{C}^{M_{\text{T}} \times C}$ and $\mathbf{b}(t) \in \mathbb{C}^{C \times 1}$ are the RF beamforming matrix and its input signal vector, respectively. In the following, we present low-complexity solutions to calculate $\mathbf{F}^{\text{opt}}(t)$ and $\mathbf{b}^{\text{opt}}(t)$ that minimize $\|\mathbf{x}_{\text{D}}(t) - \mathbf{x}_{\text{AH}}(t)\|^2$. Using (8) for RF-chain-free systems with APS, it can be easily verified that $\|\mathbf{x}_{\text{D}}(t) - \mathbf{x}_{\text{AH}}(t)\|^2 = 0$, if

$$\begin{cases} b_1^{\text{opt}}(t) = b_2^{\text{opt}}(t) = \max\limits_{m_{\text{T}}} \big|(x_{\text{D},m_{\text{T}}}(t)\big|/2, \\ F_{m_{\text{T}},1}^{\text{opt}}(t) = \mathrm{e}^{j\angle \bar{x}_{\text{D},m_{\text{T}}} + j\cos^{-1}(|\bar{x}_{\text{D},m_{\text{T}}}|)}, \\ F_{m_{\text{T}},2}^{\text{opt}}(t) = \mathrm{e}^{j\angle \bar{x}_{\text{D},m_{\text{T}}} - j\cos^{-1}(|\bar{x}_{\text{D},m_{\text{T}}}|)}, \\ b_{c\geq 3}^{\text{opt}} = 0, \\ F_{m_{\text{T}},c\geq 3}^{\text{opt}}(t) = 1, \end{cases} \tag{18}$$

where $\bar{\mathbf{x}}_{\text{D}}(t) = \mathbf{x}_{\text{D}}(t)/\max\limits_{m_{\text{T}}}\Big(\big|x_{\text{D},m_{\text{T}}}(t)\big|\Big)$. It is noted that the proposed solution is not unique, and various optimal solutions exist for this problem. When the hybrid beamformer is equipped with DPS, the optimal solutions is

$$\begin{aligned} &\big(\mathbf{F}^{\text{DPS}}(t), \mathbf{b}^{\text{DPS}}(t)\big) \\ &= \arg\min_{\mathbf{F},\mathbf{b}} \|\mathbf{x}_{\text{D}}(t) - \mathbf{x}_{\text{HA}}(t)\|^2, \\ &\quad \text{s.t. } \theta_{m_{\text{T}},c}(t) \in \{0, \ldots, (2^Q - 1)2\pi/2^Q\}, \end{aligned} \tag{19}$$

Algorithm 1 presents a low-complexity, but effective, solution for this nonconvex and combinatorial problem. Let's assume that $\mathbf{f}_1^{\text{DPS}}, \ldots, \mathbf{f}_c^{\text{DPS}}$ are known and distinct, then, we define matrix $\mathbf{F}_c = [\mathbf{f}_1^{\text{DPS}}, \ldots, \mathbf{f}_c^{\text{DPS}}]$, and vectors $\bar{\mathbf{b}}_c \in \mathbb{C}^{c\times 1}$ and $\bar{\mathbf{b}}_c^{\text{opt}} \in \mathbb{C}^{c\times 1}$, $\forall c \in \{2, \ldots, C\}$ according to

$$\bar{\mathbf{b}}_c^{\text{opt}} = \arg\min_{\bar{\mathbf{b}}_c} \|\bar{\mathbf{x}}(t) - \mathbf{F}_c\bar{\mathbf{b}}_c\|^2. \tag{20}$$

Using the least-squares approach, $\bar{\mathbf{b}}_c^{\text{opt}} = \mathbf{F}_c^{\dagger}\mathbf{x}_{\text{D}}(t)$. Similar to (11)-(13) in subsection III-B, let's define $\mathbf{w} = \bar{\mathbf{x}}_{\text{D}} - \mathbf{F}_c\bar{\mathbf{b}}_c^{\text{opt}}$. Then, we initially relax the constraint on the resolution of the phase shifters, and calculate the continuous phase values by solving

$$\begin{aligned} \mathbf{f}_{c+1}^{\text{opt}} &= \arg\min_{\mathbf{f}_{c+1}} \|\mathbf{w} - \mathbf{f}_{c+1}\|^2, \\ &\quad \text{s.t. } |F_{m_{\text{T}},c+1}| = 1, \ \angle F_{m_{\text{T}},c+1} \in [0, 2\pi) \end{aligned} \tag{21}$$

Then, we apply the quantizer function $Q(.)$ of (11), according to

$$\mathbf{f}_{c+1}^{\text{DPS}} = \mathcal{Q}(\mathbf{f}_{c+1}^{\text{opt}}). \tag{22}$$

In Algorithm 1, $\mathbf{f}_1^{\text{DPS}}$ and $\bar{b}_1^{\text{opt}} = 0.5$ are initialized by (18).

To illustrate the advantage of agile beamforming over conventional hybrid beamformers, let's consider the following example. Fig. 2 presents the achievable sum-rates by fully-digital zero-forcing (ZF), conventional hybrid beamformer of [11], and the proposed agile beamformers over a narrow-band independent and identically distributed (i.i.d.) and uncorrelated Rayleigh fading channel. When ZF is used, the received signal vector can be written as $\mathbf{y}_{\text{D}} = \mathbf{y}_{\text{D}}^{\text{Des.}} + \mathbf{z}$, where $\mathbf{y}_{\text{D}}^{\text{Des.}}$ is the desired noise-and-interference-free signal

Algorithm 1 Calculate the Beamforming Weights for Agile Hybrid Beamformer With DPS

Inputs: $\max\limits_{m_{\text{T}}}\big(|x_{\text{D},m_{\text{T}}}(t)|\big)$, $\bar{\mathbf{x}}_{\text{D}}(t) = \mathbf{x}_{\text{D}}(t)/\max\limits_{m_{\text{T}}}\big(|x_{\text{D},m_{\text{T}}}(t)|\big)$,
Calculate $\mathbf{f}_1^{\text{opt}}$ according to (18),
Calculate $\mathbf{f}_1^{\text{DPS}}(t) = \exp\Big(j\mathcal{Q}\big(\mathbf{f}_1^{\text{opt}}(t)\big)\Big)$,
Define $\mathbf{w} = \bar{\mathbf{x}}_{\text{D}}(t) - 0.5\mathbf{f}_{\text{RF},1}^{\text{DPS}}$,
for $2 \leq c \leq C$ **do**
  $\mathbf{f}_c^{\text{DPS}} = \exp\big(j\mathcal{Q}(\mathbf{w})\big)$; $\mathbf{F}_c = [\mathbf{f}_1^{\text{DPS}}, \ldots, \mathbf{f}_c^{\text{DPS}}]$; $\bar{\mathbf{b}}_c^{\text{opt}} = \mathbf{F}_c^{\dagger}(t)\bar{\mathbf{x}}_{\text{D}}(t)$; $\mathbf{w} = \bar{\mathbf{x}}_{\text{D}}(t) - \mathbf{F}_c\bar{\mathbf{b}}_c^{\text{opt}}$;
end for
Return $\mathbf{F}^{\text{DPS}}$ and $\mathbf{b}^{\text{DPS}} = \max\limits_{m_{\text{T}}}\big(|x_{\text{D},m_{\text{T}}}(t)|\big)\bar{\mathbf{b}}_C^{\text{opt}}$

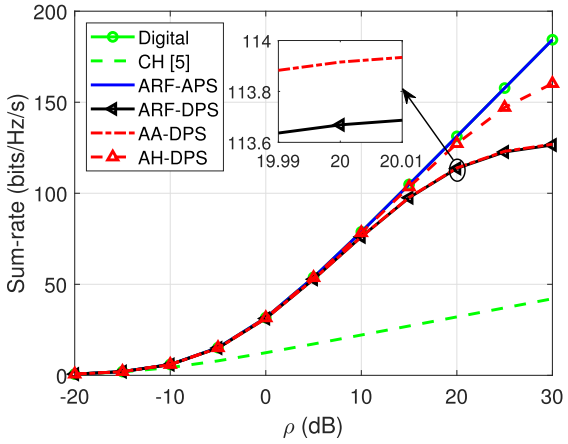

Fig. 2. Achievable sum-rates vs ρ for $T_{\text{SW}} \rightarrow 0$.

at the user equipment. The achievable sum-rate by ZF over $M_{\text{R}} \times M_{\text{T}}$ dimensional channel is expressed by [11]

$$R_{\text{D}} = M_{\text{R}} \log_2\left(1 + \mathrm{E}_{\mathbf{s}}\big[|y_{\text{D},m_{\text{R}}}^{\text{Des.}}|^2\big]/\sigma_z^2\right), \tag{23}$$

where σ_z^2 denotes the noise variance. To evaluate the performance of our proposed agile beamforming techniques, we use Gram-Schmidt process to decompose the unit vector $\hat{\mathbf{x}}_{\text{u}}$ of the transmit signal as $\hat{\mathbf{x}}_{\text{u}} = \alpha\hat{\mathbf{x}}_{\text{D}} + \sqrt{1-|\alpha|^2}\hat{\mathbf{x}}_{\text{D}}^{\perp}$, where $\alpha = \hat{\mathbf{x}}_{\text{u}}^{\text{H}}\hat{\mathbf{x}}_{\text{D}}$ is the projection of $\hat{\mathbf{x}}_{\text{u}}$ onto the direction of the desired unit vector $\hat{\mathbf{x}}_{\text{D}}$. On the other hand, $\hat{\mathbf{x}}_{\text{D}}^{\perp}$ represents the component of $\hat{\mathbf{x}}_u$ which is perpendicular to $\hat{\mathbf{x}}_{\text{D}}$. This reduces the received signal levels and can cause interference as $\hat{\mathbf{x}}_{\text{D}}^{\perp}$ points towards an undesired direction. The received signal vector can now be written as

$$\mathbf{y}_u = \mathbf{H}\mathbf{x}_u + \mathbf{z} = \|\alpha\mathbf{x}_u\|\mathbf{H}\hat{\mathbf{x}}_{\text{D}} + \sqrt{1-|\alpha|^2}\|\mathbf{x}_u\|\mathbf{H}\hat{\mathbf{x}}_{\text{D}}^{\perp} + \mathbf{z}. \tag{24}$$

Let's define $\mathbf{y}_{\text{u}}^{\text{Des.}} = \|\alpha\mathbf{x}_u\|\mathbf{H}\hat{\mathbf{x}}_{\text{D}}$ and $\mathbf{w}_u = \sqrt{1-|\alpha|^2}\|\mathbf{x}_u\|\mathbf{H}\hat{\mathbf{x}}_{\text{D}}^{\perp}$, and $\rho = P/\sigma_z^2$. By treating the undesired $\mathbf{w}_u$ as noise, the total sum-rate is

$$R_u = \sum_{m_{\text{R}}=1}^{M_{\text{R}}} \log_2\left(1 + \frac{\mathrm{E}_{\mathbf{s}}\big[|y_{u,m_{\text{R}}}^{\text{Des.}}|^2\big]}{\sigma_z^2 + \mathrm{E}_{\mathbf{s}}\big[|w_{u,m_{\text{R}}}|^2\big]}\right). \tag{25}$$

Fig. 2 presents the achievable sum-rates by the proposed agile beamformers and the conventional hybrid beamformer

of [11] with APS. The simulation parameters in Fig. 2 are $M_{\mathrm{T}} = 64$, $M_{\mathrm{R}} = 16$, $C = 3$ and $Q = 5$. It should be noted that the conventional hybrid beamformer of [11] with $C = 3$ RF-chains can only support $M'_{\mathrm{R}} = C = 3$ single-antenna users. Fig. 2 shows that even the proposed RF-chain-free beamformer with DPS can support $M_{\mathrm{R}} = 16$ users and provide a substantially higher sum-rates and spatial multiplexing gain than the conventional hybrid beamformer of [11]. It must be noted that all digital, conventional hybrid and agile RF beamformers in Fig. 2 are based on the same time-frequency resource grid. Moreover, the presented sum-rates in Fig. 2 only depend on the signal-to-interference-plus-noise ratio by the beamformer, as equation (25) indicates; and such results are independent from the specifications of the technology, e.g., the speed and capability of the baseband processor or its memory. In practical systems, however, the system designers must consider the impact of the technology limitations, such as the processing delays on the system performance. Hence, further optimization of the proposed agile RF beamforming approaches remains as a future research direction towards deploying them on hardware.

Up to this point, we have focused on agile RF beamforming approaches with infinitely fast phase shifters for RF-chain-free, analog and hybrid beamformers. Using Gram-Schmidt orthogonalization process, we analyzed the relative performance of agile approaches with respect to fully-digital ZF beamformer over a frequency-flat channel. Our analysis and simulations indicated that agile beamformers with infinitely fast phase shifters can significantly outperform conventional hybrid beamforming approaches. However, the phase shifters, in reality, have a limited response time. With this motivation, we investigate the impact of T_{SW} on the design and performance of agile beamformers in the following subsections.

E. Agile RF-Chain-Free Beamformer With Finite-Speed Phase Shifters

This subsection presents an agile RF beamforming approach for the RF-chain-free transmitter shown in Fig. 1(e) with finite-speed APS. The phase shifters switch their values at $t = (i-1)T_{\mathrm{SW}}$ and retain their phase over $(i-1)T_{\mathrm{SW}} \le t < iT_{\mathrm{SW}}$ where T_{SW} is the switching time, and i is an integer. Equation (8) can be used to replicate $\mathbf{x}_{\mathrm{D}}(t)$ only at $t = iT_{\mathrm{SW}}$, and the phase values are retained for T_{SW} after switching. In this case, (8) turns into

$$\begin{cases} f_{\mathrm{t},m_{\mathrm{T}}}(t) = \mathrm{e}^{j\angle \bar{x}_{\mathrm{D},m_{\mathrm{T}}} + j\cos^{-1}(|\bar{x}_{\mathrm{D},m_{\mathrm{T}}}|)}, & (i-1)T_{\mathrm{SW}} \le t < iT_{\mathrm{SW}} \\ f_{\mathrm{b},m_{\mathrm{T}}}(t) = \mathrm{e}^{j\angle \bar{x}_{\mathrm{D},m_{\mathrm{T}}} - j\cos^{-1}(|\bar{x}_{\mathrm{D},m_{\mathrm{T}}}|)}, & (i-1)T_{\mathrm{SW}} \le t < iT_{\mathrm{SW}}. \end{cases} \tag{26}$$

This approach can be suitable for systems that transmit signals which are in the form of pulse amplitude modulation (PAM) or amplitude shift keying (ASK). However, if $\mathbf{x}_{\mathrm{D}}(t)$ changes during $(i-1)T_{\mathrm{SW}} \le t < iT_{\mathrm{SW}}$, as in most of practical systems, using (26) results in a staircase approximation of the signal,[1] as shown in the example of Fig. 3. To model this effect, let's

[1]Such approximation may remind the reader of zero-order-hold filter.

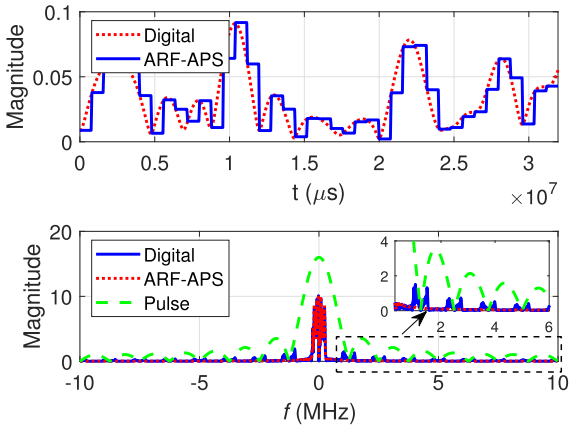

Fig. 3. Staircase approximation of a signal in (top) the time, and (bottom) frequency domains.

define the pulse function

$$p(t) = \begin{cases} 1, & t \in 0 \le t < T_{\mathrm{SW}} \\ 0, & \text{otherwise.} \end{cases} \tag{27}$$

Then, the transmit signal can be written as

$$\begin{aligned} \mathbf{x}_{\mathrm{ARF}}(t) &= \sum_{i=-\infty}^{\infty} \mathbf{x}_{\mathrm{D}}(iT_{\mathrm{SW}}) p(t - iT_{\mathrm{SW}}) \\ &= \left(\sum_{i=-\infty}^{\infty} \mathbf{x}_{\mathrm{D}}(iT_{\mathrm{SW}}) \delta(t - iT_{\mathrm{SW}}) \right) * p(t) \\ &= \mathbf{x}_{\mathrm{D}}^{(\mathrm{s})} * p(t), \end{aligned} \tag{28}$$

where $\mathbf{x}_{\mathrm{D}}^{(\mathrm{s})}(t)$ is the sampled $\mathbf{x}_{\mathrm{D}}(t)$ with a sampling frequency of $1/T_{\mathrm{SW}}$. The frequency response of $\mathbf{x}_{\mathrm{ARF}}(t)$ is

$$\begin{aligned} &\tilde{\mathbf{x}}_{\mathrm{ARF}}(f) \\ &= \tilde{\mathbf{x}}_{\mathrm{D}}^{(\mathrm{s})}(f)\tilde{p}(f) = \frac{1}{T_{\mathrm{SW}}} \sum_{l=-\infty}^{\infty} \tilde{\mathbf{x}}_{\mathrm{D}}(f - l/T_{\mathrm{SW}}) \times \tilde{p}(f) \\ &= \frac{e^{-j\pi f T_{\mathrm{SW}}} \sin\left(\pi f T_{\mathrm{SW}}\right)}{\pi f T_{\mathrm{SW}}} \times \sum_{l=-\infty}^{\infty} \tilde{\mathbf{x}}_{\mathrm{D}}(f - l/T_{\mathrm{SW}}) \\ &= e^{-j\pi f T_{\mathrm{SW}}} \mathrm{sinc}\left(f T_{\mathrm{SW}}\right) \times \sum_{l=-\infty}^{\infty} \tilde{\mathbf{x}}_{\mathrm{D}}(f - l/T_{\mathrm{SW}}). \end{aligned} \tag{29}$$

The second line in (29) expresses the relationship between the spectrum of continuous time signal and its sampled version [25]. The last equality includes the frequency response of $p(t)$. The spectrum of $\mathbf{x}_{\mathrm{D}}^{(\mathrm{s})}(t)$, denoted by $\tilde{\mathbf{x}}_{\mathrm{D}}^{(\mathrm{s})}(f)$, is a periodic function where $\tilde{\mathbf{x}}_{\mathrm{D}}(f)$ is repeated every $1/T_{\mathrm{SW}}$. Fig. 3 illustrates the time and frequency domain relationships between a band-limited $x_{\mathrm{D},m_{\mathrm{T}}}$ and its staircase approximation by the RF-chain-free beamformer. Considering (29) and the example in Fig. 3, the frequency components of $\tilde{\mathbf{x}}_{\mathrm{ARF}}(f)$ that are further away from the center tend to attenuate as $\tilde{\mathbf{x}}_{\mathrm{D}}^{(\mathrm{s})}(f)$ is multiplied with the spectrum of $p(t)$. Based on equation (29), we further discuss the consequences of the staircase approximation and design requirements for the agile RF-chain-free beamformers in the following:

1) *Signal aliasing:* Since $\tilde{\mathbf{x}}_{\mathrm{D}}^{(\mathrm{s})}(f) = \sum_{l=-\infty}^{\infty} \tilde{\mathbf{x}}_{\mathrm{D}}(f - l/T_{\mathrm{SW}})/T_{\mathrm{SW}}$ is a periodic signal, it can experience aliasing effects if $1/T_{\mathrm{SW}}$ is not large enough. Similar to Nyquist Sampling, the condition $B \leq 1/T_{\mathrm{SW}}$ must hold to avoid aliasing.
2) *Signal distortion:* As shown in Fig. 3, the spectrum of $\tilde{\mathbf{x}}_{\mathrm{D}}^{(\mathrm{s})}(f)$, around $f = 0$, is multiplied with the main lobe of a sinc function. Consequently, the signal components around the center frequency $f = 0$ are less affected by distortion. Hence, it can be deduced that narrowband signals are less susceptible to distortion and aliasing. Alternatively, using phase shifters with a smaller T_{SW} also reduces the distortion and can avoid aliasing. In addition, a filter can mitigate the signal distortion if its frequency response is in the form of

$$\begin{cases} 1/\mathrm{sinc}(T_{\mathrm{SW}} f), & -B/2 \leq f \leq B/2, \\ 0, & \text{otherwise}, \end{cases} \tag{30}$$

   To deploy this filter at the transmitter, it needs to be implemented as an analog filter and be placed before the antennas. Alternatively, analog or digital realization of this filter can be used at the receiver side.
3) *Out-of-band emissions:* As illustrated in Fig. 3 and equation (29), the spectrum of the transmit signal by the agile RF-chain-free beamformer contains undesired frequency components. The out-of-band-emissions are in the form of attenuated and distorted replicas of the spectrum of $\mathbf{x}_{\mathrm{D}}(t)$; and they are observed at the frequency bands that are centered at l/T_{SW}, where l is an integer. A low-pass filter must be used to remove the out-of-band-emissions of $\mathbf{x}_{\mathrm{ARF}}(t)$. Consequently, a band-pass filter with the same bandwidth and center frequency f_{c} is required to mitigate the undesired frequency components of $\mathbf{x}_{\mathrm{ARF}}^{\mathrm{ant.}} = \cos(2\pi f_{\mathrm{c}} t)\mathbf{x}_{\mathrm{ARF}}(t)$.
4) *Frequency-dependent phase shift*: In (29), the term $e^{j\pi f T_{\mathrm{SW}}}$ implies that the signal component at frequency f experiences a phase shift. There can be several ways to compensate for this phase shift. For example, the effect of $e^{j\pi f T_{\mathrm{SW}}}$ can be combined with the propagation channel. Then, its impact can be mitigated during channel estimation.

Based on the discussion above, the use of agile RF-chain-free beamformers with finite-speed phase shifters results in an staircase approximation of the desired transmit signal. Consequently, this can lead to signal aliasing, distortion and out-of-band emissions. To avoid signal aliasing, $B \leq 1/T_{\mathrm{SW}}$ must hold. Deploying appropriate filters can mitigate/reduce the in-band signal distortion and out-of-band emissions. Such undesired effects increase with signal bandwidth, and they decrease by using faster phase shifters. Our simulations in section IV indicate that the phase shifters' switching speed has a more dominant impact on the performance than their resolution, particularly when $Q \geq 5$. In the following subsections, we exploit the RF-chains of analog and hybrid structures to further reduce the MSEs and smooth down the transmit signal, compared to the RF-chain-free beamformer.

F. Agile Analog Beamformer With Finite-Speed Phase Shifters

This subsection presents an agile RF beamforming approach for the analog transmitter shown in Fig. 1(d) with finite-speed phase shifters. Similar to subsection III-C, let's decompose the transmit signal vector as $\mathbf{x}_{\mathrm{AA}} = b(t)\mathbf{f}(t) = b(t)(\mathbf{f}_{\mathrm{t}} + \mathbf{f}_{\mathrm{b}})/2$, and sequentially design $\mathbf{f}(t)$ and $b(t)$. The beamforming weights of $\mathbf{f}_{\mathrm{t}}(t)$ and $\mathbf{f}_{\mathrm{b}}(t)$ for $\mathbf{f}(t)$ are set according to (26). Then, the baseband weight $b^{\mathrm{opt}}(t)$ over $(i-1)T_{\mathrm{SW}} \leq t < iT_{\mathrm{SW}}$, is calculated as

$$b^{\mathrm{opt}}(t) = \arg\min_{b(t)} \Big\| \mathbf{x}_{\mathrm{D}}(t) - b(t)\mathbf{f}\big((i-1)T_{\mathrm{SW}}\big) \Big\|^2. \tag{31}$$

Similar to (16) and (17), the solution to this optimization is

$$b^{\mathrm{opt}}(t) = \big|\mathbf{x}_{\mathrm{D}}^{\mathrm{H}}\mathbf{f}\big| / \|\mathbf{f}\|^2 \exp\Big(-j\angle\big(\mathbf{x}_{\mathrm{D}}^{\mathrm{H}}\mathbf{f}\big)\Big). \tag{32}$$

This approach can be easily applied to agile analog beamformers with finite-speed DPS. Our simulations in section IV indicate that using agile analog beamformers is more advantageous over RF-chain-free systems when using phase shifters with lower-speed, and also when transmitting signals with a larger bandwidth. Next subsection investigates the design requirements and approaches for hybrid beamformers with finite-speed APS and DPS.

G. Agile Hybrid Beamformer With Finite-Speed Phase Shifters

This section presents agile RF beamforming approaches for the hybrid beamformer shown in Fig. 1(c) with finite-speed APS as well as DPS. The RF beamforming matrix $\mathbf{F}(t)$ remains constant during $(i-1)T_{\mathrm{SW}} \leq t < iT_{\mathrm{SW}}$ while its input signal $\mathbf{b}(t)$ can vary. The optimal baseband and RF beamforming weights are set such that

$$\Big(\mathbf{b}^{\mathrm{opt}}(t), \mathbf{F}^{\mathrm{APS}}\big((i-1)T_{\mathrm{SW}}\big)\Big) = \arg\min_{\mathbf{b}(t)\mathbf{F}\left((i-1)T_{\mathrm{SW}}\right)} \Big\| \mathbf{x}_{\mathrm{D}}(t) - \mathbf{F}\big((i-1)T_{\mathrm{SW}}\big)\mathbf{b}(t) \Big\|^2. \tag{33}$$

Hybrid beamformers with APS can achieve $\|\mathbf{x}_{\mathrm{D}}(t) - \mathbf{x}_{\mathrm{AH}}(t)\| = 0$, based on subsection III-D, if $\mathbf{x}_{\mathrm{D}}(t)$ remains constant during $(i-1)T_{\mathrm{SW}} \leq t < iT_{\mathrm{SW}}$. To solve (33) for a general $\mathbf{x}_{\mathrm{D}}(t)$, which varies during this interval, let's decouple the design procedure for $\mathbf{b}^{\mathrm{opt}}(t)$ and $\mathbf{F}^{\mathrm{APS}}(t)$ as in the previous subsections. Assuming that $\mathbf{F}^{\mathrm{APS}}(t)$ is available, then the least-squares approach can be used to minimize (33), i.e.,

$$\mathbf{b}^{\mathrm{opt}}(t) = \mathbf{F}^{\mathrm{APS}^{\dagger}}(t)\mathbf{x}_{\mathrm{D}}(t), \quad \forall t \in \big[(i-1)T_{\mathrm{SW}}, iT_{\mathrm{SW}}\big). \tag{34}$$

It is desired to construct a full-ranked $\mathbf{F}^{\mathrm{APS}}(t)$ to increase the degrees of freedom of the hybrid beamformer. When using APS, Algorithm 2 presents our approach to construct a full-ranked $\mathbf{F}^{\mathrm{APS}}$ for a general $\mathbf{x}_{\mathrm{D}}(t)$, which varies during $t \in \big[(i-1)T_{\mathrm{SW}}, iT_{\mathrm{SW}}\big)$. It is noted that this solution is not unique, and further optimization of this algorithm for specific waveforms of interest remains as a future research

Algorithm 2 Constructing a Full-Ranked $\mathbf{F}^{\text{APS}}(t)$ for Agile Hybrid Beamformers With APS

Input: C, i and $\mathbf{x}_{\text{D}}(t)$ where $t \in [0, 2\pi)$,
Define $\bar{\mathbf{x}}_{\text{D}}(t) = \mathbf{x}_{\text{D}}(t)/\max_{t,m_{\text{T}}}\big(|x_{\text{D},m_{\text{T}}}(t)|\big)$; Define $\bar{C} = \lceil C/2 \rceil$; Define $t_{i,\bar{c}} \in \big[(i-1)T_{\text{SW}}, iT_{\text{SW}}\big)$ such that $\mathbf{x}_{\text{D}}(t_{i,\bar{c}}) \neq \mathbf{x}_{\text{D}}(t_{i,\bar{c}'})$, $\forall \bar{c}, \bar{c}' \in \{1, \ldots, \bar{C}\}$
for $1 \leq \bar{c} \leq \bar{C} - 1$ **do**
  $F^{\text{APS}}_{m_{\text{T}},2\bar{c}-1}(t) = \text{e}^{j\angle \bar{x}_{\text{D},m_{\text{T}}}(t_{i,\bar{c}}) + j\cos^{-1}(|\bar{x}_{\text{D},m_{\text{T}}}(t_{i,\bar{c}})|)}$
  $F^{\text{APS}}_{m_{\text{T}},2\bar{c}}(t) = \text{e}^{j\angle \bar{x}_{\text{D},m_{\text{T}}}(t_{i,\bar{c}}) - j\cos^{-1}(|\bar{x}_{\text{D},m_{\text{T}}}(t_{i,\bar{c}})|)}$
end for
if $C = 2\bar{C}$ **then**
  $F^{\text{APS}}_{m_{\text{T}},2\bar{C}-1}(t) = \text{e}^{j\angle \bar{x}_{\text{D},m_{\text{T}}}(t_{i,\bar{C}}) + j\cos^{-1}(|\bar{x}_{\text{D},m_{\text{T}}}(t_{i,\bar{C}})|)}$
  $F^{\text{APS}}_{m_{\text{T}},2\bar{C}}(t) = \text{e}^{j\angle \bar{x}_{\text{D},m_{\text{T}}}(t_{i,\bar{C}}) - j\cos^{-1}(|\bar{x}_{\text{D},m_{\text{T}}}(t_{i,\bar{C}})|)}$
else
  if $C = 2\bar{C} - 1$ **then**
    $F^{\text{APS}}_{m_{\text{T}},C}(t) = e^{j\angle \bar{x}_{\text{D},m_{\text{T}}}(t_{i,\bar{C}})}$
  end if
end if
Return $\mathbf{F}^{\text{APS}}\big((i-1)T_{\text{SW}} \leq t < iT_{\text{SW}}\big)$

direction. Let's consider two scenarios where C is either an even or an odd number. If the number of RF-chains C is even, define $\bar{C} = C/2$; otherwise, $\bar{C} = (C+1)/2$. Then, select $\bar{C}$ samples of the signal such that $\mathbf{x}_{\text{D}}(t_{i,\bar{c}}) \neq \mathbf{x}_{\text{D}}(t_{i,\bar{c}'})$ for $\bar{c} \neq \bar{c}'$, where $t_{i,\bar{c}}, t_{i,\bar{c}'} \in \big[(i-1)T_{\text{SW}}, iT_{\text{SW}}\big)$, $\forall \bar{c}, \bar{c}' \in \{1, 2, \ldots, \bar{C}\}$ and $t_{i,1} = (i-1)T_{\text{SW}}$. If T_{SW} is sufficiently small and $\Big|x_{\text{D},m_{\text{T}}}\big((i-1)T_{\text{SW}} \leq t < iT_{\text{SW}}\big)\Big|$ is a strictly increasing/decreasing function, then $t_{i,\bar{c}}$ can be simply chosen by uniformly dividing $\big[(i-1)T_{\text{SW}}, iT_{\text{SW}}\big)$ into $\bar{C}$ intervals, as $\mathbf{x}_{\text{D}}(t_{i,\bar{c}}) \neq \mathbf{x}_{\text{D}}(t_{i,\bar{c}'})$ for $\bar{c} \neq \bar{c}'$ holds. Consequently, it can be easily verified that $\mathbf{F}^{\text{APS}}(t)$, $\forall t \in \big[(i-1)T_{\text{SW}}, iT_{\text{SW}}\big)$, is a full-ranked matrix by setting its elements as

$$\begin{cases} F^{\text{APS}}_{m_{\text{T}},2\bar{c}-1}(t) = \text{e}^{j\angle \bar{x}_{\text{D},m_{\text{T}}}(t_{i,\bar{c}}) + j\cos^{-1}(|\bar{x}_{\text{D},m_{\text{T}}}(t_{i,\bar{c}})|)}, \\ F^{\text{APS}}_{m_{\text{T}},2\bar{c}}(t) = \text{e}^{j\angle \bar{x}_{\text{D},m_{\text{T}}}(t_{i,\bar{c}}) - j\cos^{-1}(|\bar{x}_{\text{D},m_{\text{T}}}(t_{i,\bar{c}})|)}, \end{cases} \tag{35}$$

when C is an even number. If $C = 2\bar{C} - 1$, we use (35) for $\bar{c} \in \{1, \ldots, \bar{C}-1\}$, and set the last column of $\mathbf{F}^{\text{APS}}$ according to $\arg\min_{\mathbf{f}_C} \|\bar{\mathbf{x}}_{\text{D}}(t_{i,\bar{C}}) - \mathbf{f}_{\text{C}}(t)\|^2$, which results in

$$F^{\text{APS}}_{m_{\text{T}},C}(t) = e^{j\angle \bar{x}_{\text{D},m_{\text{T}}}(t_{i,\bar{C}})}. \tag{36}$$

For hybrid beamformers with DPS, it can be easily verified that a full-ranked $\mathbf{F}^{\text{DPS}}(t)$ can be constructed by using Algorithm 1, with $\mathbf{x}_{\text{D}}((i-1)T_{\text{SW}})$ as its input. Then, $\mathbf{b}^{\text{DPS}}(t)$ can be set according to the least-squares solution, similarly to (34).

In this subsection, we presented agile RF beamforming methods for hybrid beamformers with finite-speed phase shifters. In our approach, the RF beamforming matrix is created based on Algorithm 1 and Algorithm 2 for hybrid beamformers with DPS and APS, respectively. The baseband beamforming weights are, then, calculated using the least-squares approach as in (34). Our simulations results in section IV indicate that the proposed agile hybrid beamformers can substantially improve the performance, compared to RF-chain-free and analog beamformers.

IV. Simulation Results

In this section, first we introduce metrics to simulate and evaluate the performance of the proposed agile beamformers in terms of normalized MSE, in-band distortion, out-of-band emissions, and relative signal loss compared to the desired reference signal. More specifically, in subsection IV-A, we investigate the impact of phase shifters' switching time T_{SW} and resolution Q, signal's bandwidth $B = \tilde{K}\Delta f$, and the number of transmitter antennas M_{T} on the performance of agile beamformers. Then, in subsection IV-B, we present three examples in the context of wireless communication systems to provide more insights about the performance of the proposed approaches. In particular, we focus on the impact of T_{SW} on ACLR, achievable sum-rates and power efficiency compared to the conventional hybrid beamformers, RMS EVM of 64-QAM constellation and the BER.

A. Evaluating the Relative Performance of Agile RF Beamformers Compared to the Reference Signal

In this subsection, we use Monte-Carlo simulations averaged over 1000 realizations to evaluate the normalized MSE, signal loss, in-band signal distortion, and out-of-band emissions of the signals compared to the desired signal $\mathbf{x}_{\text{D}}(t)$. The band-limited baseband signal $\tilde{\mathbf{x}}^{\text{Base.}}_{\text{D}}(k)$ with $\tilde{K}$ nonzero subcarriers is created such that $\tilde{x}^{\text{Base.}}_{\text{D},m_{\text{T}}}(k) \sim \mathcal{CN}(0,1)$, $\forall k \in \{\pm 1, \pm 2, \ldots, \pm\tilde{K}/2\}$ where $\tilde{K}$ is assumed to be an even number. After converting the baseband signal to a low-pass signal, the transmit power of $\mathbf{x}_u(t)$ is normalized such that $\sum_{m_{\text{T}}=1}^{M_{\text{T}}} \int_0^{KT_{\text{s}}} \|x_{u,m_{\text{T}}}(t)\|^2 \, dt = 1$, where $T_{\text{S}} = 1/K\Delta f$ is the sampling period of the baseband signal. To simulate the continuous-time transmit signal $\mathbf{x}_u(t)$, we construct a corresponding discrete signal $\mathbf{x}_u(iT_{\text{DAC}})$ by upsampling $\mathbf{x}^{\text{Base.}}_u(iT_{\text{S}})$ where $T_{\text{DAC}} \ll T_{\text{S}}$. To simulate infinitely fast phase shifters with $T_{\text{SW}} \to 0$, we assume that the phase shifters are updated every T_{DAC}. Except otherwise is stated, the simulation parameters are set as $T_{\text{SW}} = 0.5/T_{\text{s}}$, $\tilde{K} = 16$, $K = 32$, $M_{\text{T}} = 64$, $Q = 5$, and the upsampling factor is $T_{\text{SW}}/T_{\text{DAC}} = 10$ for all systems. In addition, the number of RF chains for the hybrid structures is set to $C = 2$.

Fig. 4 presents the impact of $\tilde{K}$, Q, $T_{\text{SW}}/T_{\text{s}}$, and M_{T} on the normalized MSE per antenna over a time interval of duration T_{s}. In particular, we calculate the normalized MSE according to

$$e_u = \frac{\int_0^{KT_{\text{s}}} \|\mathbf{x}_{\text{D}}(t) - \mathbf{x}_u(t)\|^2 dt}{\int_0^{KT_{\text{s}}} \|\mathbf{x}_{\text{D}}(t)\|^2 dt}. \tag{37}$$

When $Q \geq 5$ bits, Fig. 4(a) shows that the performance of agile beamformers with DPS is almost the same as using APS. It should be noted that the structures that employ APS serve as a benchmark in Fig. 4(a) considering that the resolution of APS does not change over the horizontal axis. Fig. 4(a) indicates that the RF-chain-free systems are more sensitive to the resolution of the phase shifters, compared with other

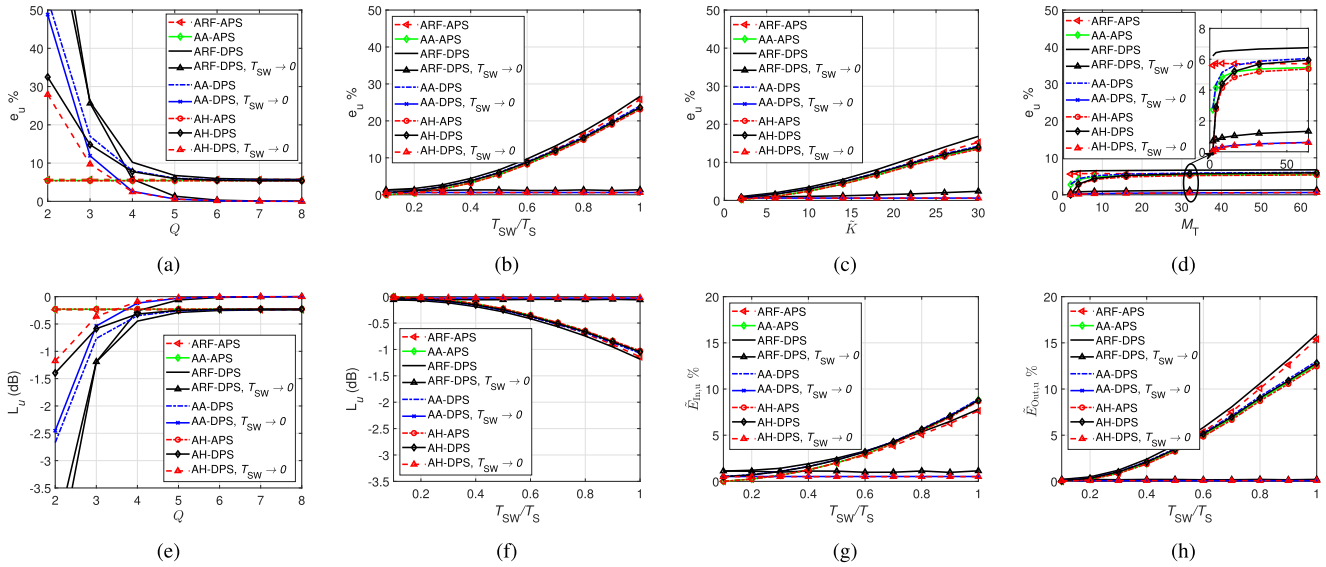

Fig. 4. (a) e_u v.s. Q, (b) e_u v.s. $T_{\text{SW}}/T_{\text{S}}$, (c) e_u v.s. $\tilde{K}$, (d) e_u v.s. M_{T}, (e) L_u v.s. Q, (f) L_u v.s. $T_{\text{SW}}/T_{\text{S}}$, (g) $\tilde{E}_{\text{In},u}$ v.s. $T_{\text{SW}}/T_{\text{S}}$, (h) $\tilde{E}_{\text{Out},u}$ v.s. $T_{\text{SW}}/T_{\text{S}}$.

methods. As the resolution of the phase shifters increases, the normalized MSE of the beamformers with finite-speed phase shifters reaches an error floor. Hence, Fig. 4(a) indicates that T_{SW} has a more substantial impact on e_u than Q.

Fig. 4(b) presents the impact of $T_{\text{SW}}/T_{\text{s}}$ on the normalized MSE. It is noted that the approaches that are based on infinitely fast phase shifters, i.e. $T_{\text{SW}} \to 0$, serve as performance benchmark as their switching speed does not vary along the horizontal axis. For system u, Fig. 4(b) indicates that using DPS, instead of APS with the same speed, increases the MSE by only a small offset, while the corresponding curves follow a similar slope. Fig. 4(b) shows that the slope of MSE for the analog beamformer is significantly reduced compared to the RF-chain-free system. Similarly, a hybrid beamformer with $C = 2$ can further reduce the slope of MSE. Fig. 4(b) indicates that all structures achieve a similar performance when faster phase shifters are deployed.

Fig. 4(c) presents the impact of $\tilde{K}$ on e_u, showing that the MSE is relatively negligible when $T_{\text{SW}} \to 0$. For example, the normalized MSE by the agile hybrid beamformer e_{AH} with DPS is less than 1%, regardless of the bandwidth of the signal. The performance of agile beamformers, with finite-speed phase shifters, degrades as the bandwidth increases. Similar to Fig. 4(b), using DPS results in a small performance loss compared with APS. Moreover, additional RF-chains significantly reduce the slope of the MSE.

Fig. 4(d) shows the impact of the number of antennas on the normalized MSE per antenna element. When $T_{\text{SW}} \to 0$, Fig. 4(d) indicates that Q has a more significant impact on e_u than the number of antennas. When the phase shifters have a finite switching speed, increasing the number of antennas initially increases the relative MSE per antenna; however, the MSE almost saturates when $M_{\text{T}} \geq 16$. In addition, the MSE appears to be less sensitive to M_{T}, for $Q \geq 5$ than T_{SW} and $\tilde{K}$.

To examine the spectrum of the transmit signals, we define the signal loss, normalized in-band and out-of-band errors between the $\mathbf{x}_{\text{D}}(t)$ and $\mathbf{x}_u(t)$ using Gram-Schmidt orthogonalization process. The m_{T}-th element of $\mathbf{x}_u(t)$ can be decomposed as

$$x_{u,m_{\text{T}}}(t) = \eta_{u,m_{\text{T}}} x_{\text{D},m_{\text{T}}}(t) + e^{\perp}_{u,m_{\text{T}}}(t) \tag{38}$$

where $\eta_{u,m_{\text{T}}}$ corresponds to the projection of $x_{u,m_{\text{T}}}(t)$ onto $x_{\text{D},m_{\text{T}}}(t)$, and $e^{\perp}_{u,m_{\text{T}}}(t)$ is an orthogonal function to $x_{\text{D},m_{\text{T}}}$. In (38), $\eta_{u,m_{\text{T}}} x_{\text{D},m_{\text{T}}}(t)$ and $e^{\perp}_{u,m_{\text{T}}}(t)$ can be interpreted as the desired and undesired components of $x_{u,m_{\text{T}}}(t)$ compared to $x_{\text{D},m_{\text{T}}}(t)$, respectively. Using Gram-Schmidt procedure,

$$\begin{cases} \eta_{u,m_{\text{T}}} = \dfrac{\int_0^{KT_{\text{s}}} x_{u,m_{\text{T}}}(t) x^*_{\text{D},m_{\text{T}}}(t) dt}{\int_0^{KT_{\text{s}}} |x_{\text{D},m_{\text{T}}}(t)|^2 dt} \\ e^{\perp}_{u,m_{\text{T}}}(t) = x_{u,m_{\text{T}}}(t) - \eta_{u,m_{\text{T}}} x_{\text{D},m_{\text{T}}}(t). \end{cases} \tag{39}$$

Based on (39), let's define $\mathcal{B} = [-\tilde{K}\Delta f/2, \tilde{K}\Delta f/2]$ and

$$\begin{cases} L_u = \text{E}_{m_{\text{T}}}\left[|\eta_{u,m_{\text{T}}}|^2\right] \\ \tilde{E}_{\text{In},u} = \text{E}_{m_{\text{T}}}\left[\dfrac{\int_{f\in\mathcal{B}} |\tilde{e}^{\perp}_{u,m_{\text{T}}}(f)|^2 \, df}{\int_{-\infty}^{\infty} |\tilde{x}_{u,m_{\text{T}}}(f)|^2 \, df}\right], \\ \tilde{E}_{\text{Out},u} = \text{E}_{m_{\text{T}}}\left[\dfrac{\int_{f\notin\mathcal{B}} |\tilde{e}^{\perp}_{u,m_{\text{T}}}(f)|^2 \, df}{\int_{-\infty}^{\infty} |\tilde{x}_{u,m_{\text{T}}}(f)|^2 \, df}\right], \end{cases} \tag{40}$$

where L_u, $\tilde{E}_{\text{In},u}$ and $\tilde{E}_{\text{Out},u}$ are a measure of signal loss in the desired direction, undesired in-band distortion and out-of-band emissions, respectively.

Fig. 4(e) shows that the signal loss L_u is within a 0.5 dB margin by all methods if $Q \geq 4$. In addition, L_u decreases as the speed of the phase shifters reduces, i.e., T_{SW} increases. Fig. 4(f) indicates T_{SW} and C have a more substantial impact on L_u than Q. In Fig. 4(f), the agile RF-chain-free beamformer with DPS and $T_{\text{SW}}/T_{\text{s}} = 1$ has only around 1 dB loss. For a given bandwidth, Fig. 4(g) and Fig. 4(h) indicate that both the in-band and out-of-band emissions increase as T_{SW} increases.

On the other hand, increasing the number of the RF-chains significantly reduces the slop of $\tilde{E}_{\text{In},u}$ and $\tilde{E}_{\text{Out},u}$.

B. Evaluating Agile RF Beamformers in Communication Systems

This subsection evaluates the impact of the phase shifter's resolution and speed on the performance of agile RF beamforming in terms of ACLR, sum-rate, power efficiency, EVM and BER. For the sake of clarity, we use three different examples to better investigate the aforementioned parameters. It is noted that Q and T_{SW} in practical systems significantly depend on the technology of the phase shifters [26]. While the resolution of the digital phase shifters can be as low as a few bits, phase shifters with 6-bits of resolution, or even higher, are commonly used in practice [7]. In terms of the switching speed, the phase phase shifter's that are based on monolithic microwave integrated circuit (MMIC) can be as fast as $T_{\text{SW}} \leq 1$ ns, whereas $10\mu\text{s} \leq T_{\text{SW}} \leq 100\mu\text{s}$ for micro electro-mechanical systems (MEMS) technology [26]. Digital phase shifters can be programmed in parallel and/or serial modes which also has an impact on the switching speed of the phase shifters. It is noted that using the parallel mode to control the phase shifters with higher resolution can improve the switching time of the phase shifters at the cost of more complex circuitry. Hence, in the following, we will consider several values for T_{SW} to better investigate the impact of T_{SW} on the system performance. It must be noted that the key indicator for the performance of the agile beamformers is the relative value of $T_{\text{SW}}B$ rather than the independent values of T_{SW} and B and the carrier frequency. Hence, the following results and trends can be extended to any other frequency band as long as the relative values of T_{SW} and T_{S} remain the same.

Example 1: This example presents the impact of power amplifier's nonlinearities, Q, T_{SW} and the use of filtering on the spectrum of the transmit signal and the corresponding ACLR. ACLR is defined as the ratio of the mean filtered power in the desired band to the mean filtered power in the adjacent frequency channel, and it is one of the common metrics in the study of the out-of-band emissions in wireless systems. In this example, we use 5G and Communication toolboxes of MATLAB [27] to create 5G new radio (NR) test models (TM) for the frequency range 1 (FR1) [28] and to introduce the nonlinear impact of the power amplifier using Rapp model [29]. The TMs are defined by 3rd generation partnership (3GPP), and are used for conformance testing in specific 3GPP supported RF configurations. In the following, $\mathbf{x}_{\text{D}}(n)$ is produced based on NR-FR1-TM1.1 using time-division duplex (TDD) mode with $B = 20$ MHz, $\Delta f = 30$ kHz; and the nonlinearity effects are created based on Rapp model with smoothness factor set to 2. Fig. 5 compares the spectrum and ACLR of the transmit signal from a single-antenna digital transmitter to that of an RF-chain-free system. It is noted that, in the following, we only focus on low-pass signal models; and consequently, the corresponding filters are low-pass filters. Considering the power amplifier's nonlinearity, Fig. 5(a)-Fig. 5(d) indicate that the use of filters improves the ACLR performance of digital transmitters. On the other hand, Fig. 5(e)-Fig. 5(l) indicate that it is critical for the RF-chainfree systems with finite-speed analog phase shifters to apply filters before the antennas. More specifically, Fig. 5(e)-Fig. 5(l) present the spectrum and ACLR of unfiltered and filtered signals when $T_{\text{SW}} = 32.5$ ns and $T_{\text{SW}} = 24.4$ ns. It is observed that all other channels experience a dramatic interference, and the ACLR reaches unexpected levels if a filter is not used. Using faster analog phase shifters, i.e., $T_{\text{SW}} = 24.4$ ns, Fig. 5(i)-Fig. 5(l) show that although there is no interference on the adjacent channels, labeled with "-1" and "1", channels "-2" and "2" are significantly affected. Hence, Fig. 5(e)-Fig. 5(l) indicate that the use of faster analog phase shifters can relax the design constraints of the filter. However, it does not alleviate the need for low-pass filters. Fig. 5(m)-Fig. 5(p) investigate the impact of very fast digital phase shifting on the spectrum and ACLR. In this scenario, there is significant leakage to other frequency-bands and the use of filters is inevitable regardless of T_{SW}.

Example 2: This example evaluates the impact of T_{SW} on the achievable sum-rates and power efficiency of the agile RF beamforming compared to fully-digital, and conventional RF beamforming approach of [12] for a point-to-point MIMO systems. To provide an insight about the performance of agile RF beamforming in mmWave channels, in the following, we consider a sparse scattering geometry-based channel model where the channel matrix $\mathbf{H}$ is described by [12]

$$\mathbf{H} = \sqrt{\frac{M_{\text{T}}M_{\text{R}}}{N_{\text{cl}}N_{\text{ray}}}} \sum_{i=1}^{N_{\text{cl}}} \sum_{j=1}^{N_{\text{ray}}} g_{i,j} \Lambda_{\text{R}}(\phi_{i,j}^{\text{R}}, \psi_{i,j}^{\text{R}}) \Lambda_{\text{T}}(\phi_{i,j}^{\text{T}}, \psi_{i,j}^{\text{T}}) \times \mathbf{a}_{\text{R}}(\phi_{i,j}^{\text{R}}, \psi_{i,j}^{\text{R}}) \mathbf{a}_{\text{T}}^{\text{H}}(\phi_{i,j}^{\text{T}}, \psi_{i,j}^{\text{T}}). \quad (41)$$

In this model, N_{cl}, N_{ray}, $g_{i,j}$, Λ_{R}, $\phi_{i,j}^{\text{R}}$ and $\psi_{i,j}^{\text{R}}$, $\mathbf{a}_{\text{R}}$ denote the total number clusters, the number of the rays in each cluster, the corresponding path coefficient, receiver antenna pattern, the azimuth and elevation angle-of-arrival, the array response vector of the receiver, respectively. Similar notation and terminology is used for the transmitter side. It is noted that mmWave channels can show several hundreds of coherence bandwidth in some realistic environments, in particular when a directional transmission is used [30]. Hence, the model in (41) is still a viable model to evaluate the transmission of signals with a relatively large bandwidth in mmWave scenarios. Consequently, the frequency-response of the channel at the k-th, $k \in \{0, 1, \ldots, K-1\}$, subcarrier is equal to $\mathbf{H}$. To better focus on the performance of the transmitters, we further assume that the multiantenna receiver is equipped with a fully-digital array.

In the following, we assume the transmission scheme is based on singular value decomposition of $\mathbf{H}$ without using waterfilling [11], [12]. More precisely, let $\mathbf{H} = \mathbf{U}\mathbf{\Sigma}\mathbf{V}^{\text{H}}$ where $\mathbf{U} \in \mathbb{C}^{M_{\text{R}} \times M_{\text{R}}}$ and $\mathbf{V} \in \mathbb{C}^{M_{\text{T}} \times M_{\text{T}}}$ are unitary matrices including the left and right singular vectors, and the diagonal elements of $\mathbf{\Sigma} \in \mathbb{C}^{M_{\text{R}} \times M_{\text{T}}}$ contain the singular values of $\mathbf{H}$. It is noted that both digital and agile RF beamformers can support the transmission of up to $M_{\text{U}} = \min(M_{\text{T}}, M_{\text{R}})$ data streams. However, we impose $M_{\text{U}} = C$ limitation, where C is the number of the RF chains of a conventional hybrid beamformer, to make comparisons with conventional hybrid beamforming approaches in similar scenarios. Accordingly,

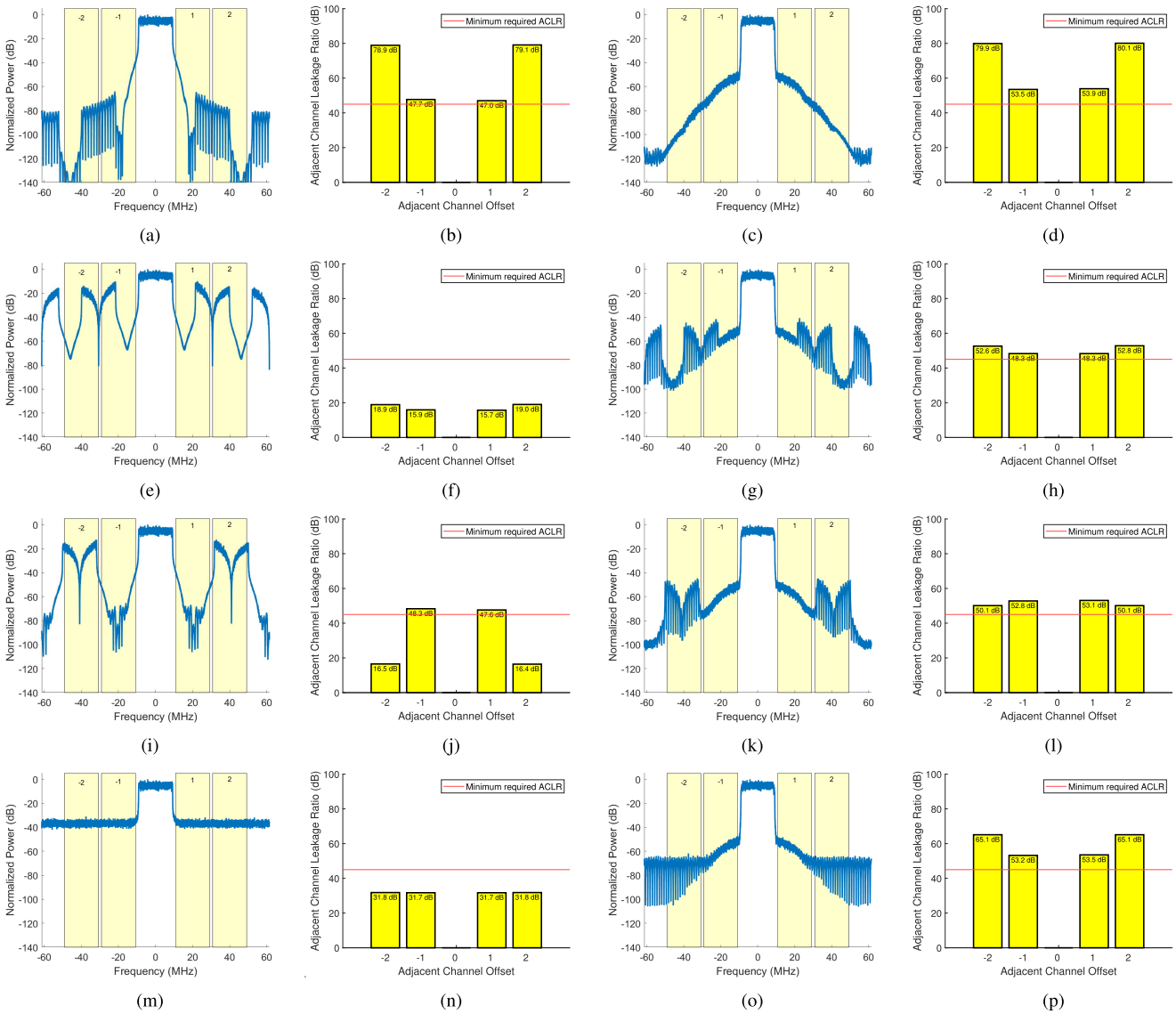

Fig. 5. Spectrum and ACLR of: (a), (b) digital transmitter without filter, (c), (d) with filter; (e), (f) ARF with APS $T_{\text{SW}} = 32.5$ ns without filter, (g), (h) with filter, (i), (j) ARF with APS $T_{\text{SW}} = 24.4$ ns without filter, (k), (l) with filter, (m), (n) ARF with DPS $Q = 6$, $T_{\text{SW}} \to 0$ ns, (o), (p) without filter.

the precoding and combining matrices for a digital system are set as $\mathbf{F}_{\text{D}} = \mathbf{V}_{1:M_{\text{U}}}$ and $\mathbf{W}_{\text{D}} = \mathbf{U}^{\text{H}}_{1:M_{\text{U}}}$. Based on $\mathbf{F}_{\text{D}}$ and $\mathbf{W}_{\text{D}}$, we adopt the precoding approach of [12] to calculate the achievable rates by conventional hybrid beamformers to calculate $\mathbf{F}_{\text{CH}} = \mathbf{F}_{\text{CH}}\mathbf{B}_{\text{CH}}$. Let $\tilde{s}_{m_{\text{U}}}(k)$, $m_{\text{U}} \in \{1, 2, \ldots, M_{\text{U}}\}$ be a zero-mean Gaussian random variable with unit variance, and denote the m_{U}-th symbol on the k-th subcarrrier. Based on the outcomes of Example 1, we investigate the impact of analog signals by upsampling and filtering the baseband signals.

For band-limited signals and additive zero-mean Gaussian noise with normalized unit-variance, the achievable sum-rate over $\mathbf{H}$ is [10], [31]

$$R_u = \frac{1}{K}\sum_{0}^{K-1} \log_2 \det\left(\mathbf{I} + \mathbf{H}\mathbf{Q}_{\tilde{\mathbf{x}}_u}(k)\mathbf{H}^{\text{H}}\right), \tag{42}$$

where $\mathbf{Q}_{\tilde{\mathbf{x}}_u}(k)$ denotes the covariance matrix of the $\tilde{\mathbf{x}}_u(k)$. It must be noted that the discrete variable $\tilde{\mathbf{x}}_u(k)$ is created from the contentious-time $\mathbf{x}_u(t)$, and it must comply with Nyquist sampling criteria before it is used in (42). In this example, we also evaluate the power efficiency $R_u/P_{\text{tot},u}$ of different approaches, where $P_{\text{tot},u}$ is the total power consumption of the transmitter that is used for achieving R_u [32]. The calculation of $P_{\text{tot},u}$ is based on the hardware configurations shown in Fig. 1, and based on the parameters used in [32], [33]. For the digital transmitter, $P_{\text{tot,Dig}} = M_{\text{T}}(P_{\text{A}} + P_{\text{RFC}}) + P_{\text{BB}}$ where $P_{\text{A}} = 20$ mW, $P_{\text{RFC}} = 230$ mW and $P_{\text{BB}} = 5$ mW denote the power consumption of power amplifiers, RF chains and baseband, respectively. For the hybrid beamformer with C RF chains, $P_{\text{tot,CH}} = M_{\text{T}}(C+1)P_{\text{A}} + M_{\text{T}}CP_{\text{SW}} + CP_{\text{RFC}} + P_{\text{BB}}$ where $P_{\text{SW}} = 30$ mW denotes the power consumption of the phase shifters. For the agile RF-chain-free and analog beamformers, each phase shifter and antenna are assumed to be equipped with power amplifiers. Since each antenna is connected to two phase shifters, we model the power

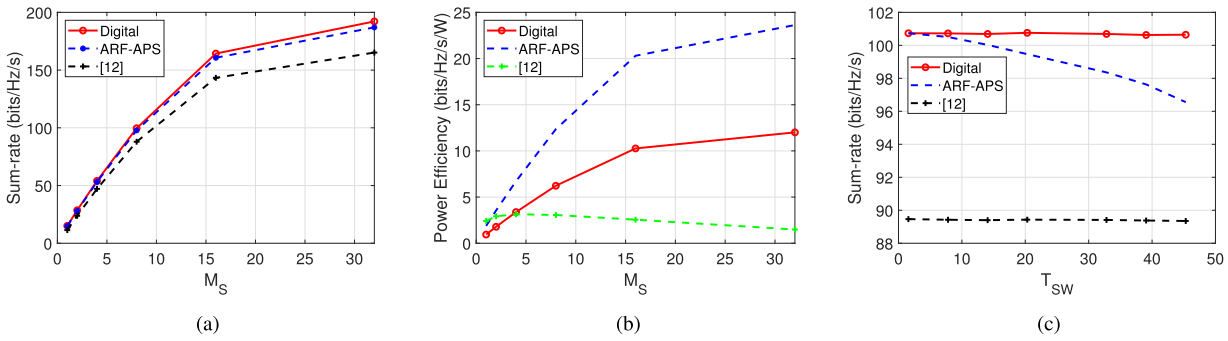

Fig. 6. (a) Achievable sum-rate vs $M_{\rm s} = M_{\rm U}$, (b) power efficiency vs $M_{\rm s}$, (c) achievable sum-rate vs $T_{\rm SW}$.

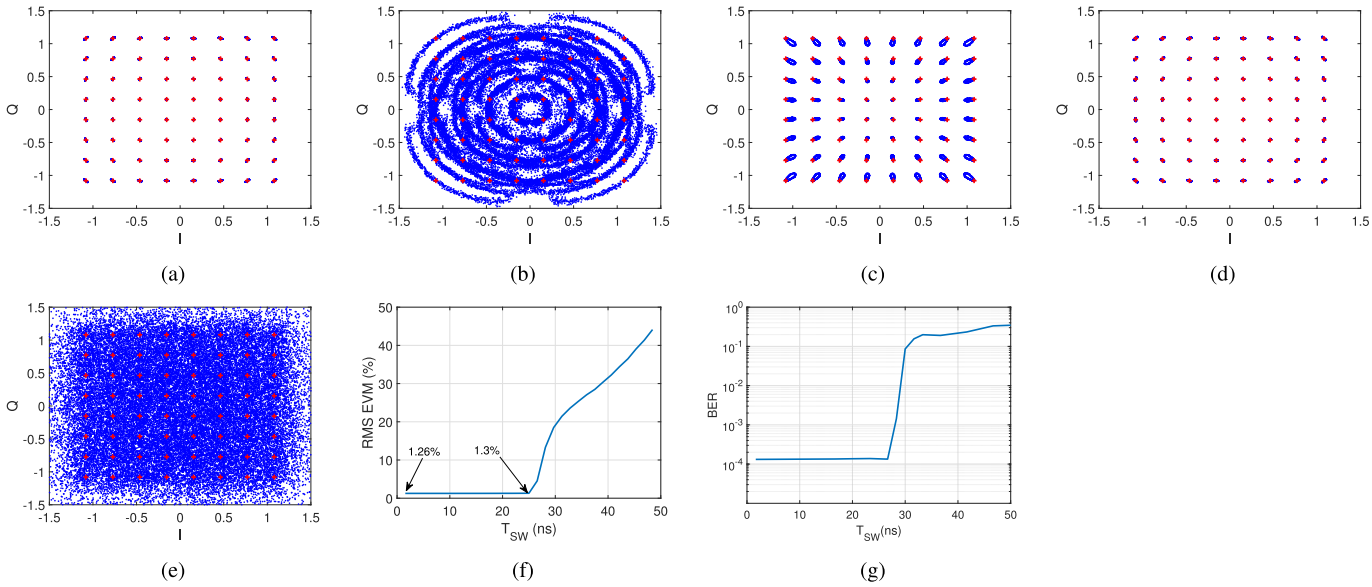

Fig. 7. Signal constellation for (a) $T_{\rm SW} = 1.5$ ns with no compensation, (b) $T_{\rm SW} = 25$ ns with no compensation, (c) $T_{\rm SW} = 25$ ns with phase compensation, (d) $T_{\rm SW} = 25$ ns with phase and amplitude compensation, (e) $T_{\rm SW} = 47$ ns with phase and amplitude compensation, (f) RMS EVM vs $T_{\rm SW}$, (g) BER vs $T_{\rm SW}$.

consumption of the system based on $P_{\rm tot,ARF} \approx P_{\rm tot,AA} = 3M_{\rm T}P_{\rm A} + 2M_{\rm T}P_{\rm SW} + P_{\rm RFC} + P_{\rm BB}$.

Fig. 6 presents the simulation results for the sum-rates v.s. $M_{\rm U} = C$, power efficiency v.s. $M_{\rm U}$ and the sum-rate v.s. $T_{\rm SW}$. The transmitter and receiver have uniform rectangular arrays with 64 omnidirectional antennas, $N_{\rm cl} = M_{\rm U}$ is set such that the rank of the channel matrix can support the transmission of $M_{\rm U}$ data streams, $N_{\rm ray} = 5$, $\phi^{\rm R}_{i,j} \in [-90°, 90°,]$, $\psi^{\rm R}_{i,j} \in [-45°, 45°,]$, $\phi^{\rm T}_{i,j} \in [-30°, 30°,]$, $\psi^{\rm R}_{i,j} \in [-10°, 10°,]$, $\rho = {\rm E}\big[{\rm trace}(\mathbf{F}_{\rm CH}\mathbf{F}^{\rm H}_{\rm CH})\big]/\sigma^2_{\rm z} = {\rm E}\big[{\rm trace}(\mathbf{F}_{\rm D}\mathbf{F}^{\rm H}_{\rm D})\big]/\sigma^2_{\rm z}$, $B = 20$ MHz. Fig. 6(a) indicates that the proposed agile RF-chain-free beamformer with $T_{\rm SW} = 25$ ns and the digital transmitter provide a similar performance which is still comparable to that of the conventional hybrid beamformer. However, Fig. 6(b) shows that the RF-chain-free system offers significantly higher power efficiency than both digital and conventional hybrid beamformers as the number of the transmit streams increases. It is noted that in such scenarios conventional hybrid beamformers consume much higher power even compared to digital systems [13], [24]. Fig. 6(c) presents the achievable sum-rates by the agile RF-chain-free beamformer, where $M_{\rm U} = 8$, reduces as $T_{\rm W}$ increases. It is observed that even for $T_{\rm SW} = 47$ ns $\approx 1/B = 50$ ns, the agile beamformer provides higher sum-rates than the conventional hybrid beamformer.

Example 3: This example investigates the impact of $T_{\rm SW}$ on the signal constellation, EVM and BER of the proposed approach. In general, the BER and EVM in wireless systems depend on various parameters, e.g., signal-to-noise ratio, the choice of modulation and coding scheme, the nonlinearities of the circuit components, the time dispersive characteristics and the rank of the MIMO channel. To decouple the impact of $T_{\rm SW}$ on the signal constellation, BER and EVM from the aforementioned variables, we confine the scope of this example to a simplified scenario where $M_{\rm T} = M_{\rm R} = 8$ over $\mathbf{H} = \mathbf{I}_{M_{\rm T}}$. In this example, the transmit signal on the k-th subcarrier, from each antenna is based on 64-quadrature-amplitude-modulation (64-QAM). Similar to the previous examples, the baseband signal is upsampled and filtered before transmission, and the receiver applies the same sampling frequency $T_{\rm S} = 1/B$ where $B = 20$ MHz. To better elaborate on the impact of $T_{\rm SW}$ on the signal constellation and EVM of signal, Fig. 7(a)-Fig. 7(f) consider a noise free scenario. Fig. 7(a) indicates that the signal constellation of digital and agile RF beamformer are nearly the same when $T_{\rm SW} = 1.5$ ns. As expected from

subsection III-E, Fig. 7(b) shows that the signal constellation experiences a significant phase rotation and signal distortion when $T_{\text{SW}} = 25$ ns. The receiver of Fig. 7(c) applies an appropriate time-offset before downsampling to compensate for the phase rotation. To overcome the amplitude distortion of the constellation in Fig. 7(c), the transmitter of Fig. 7(d) preprocesses the transmit signal according to (30). However, as Fig. 7(e) and Fig. 7(f) indicate, more efficient approaches are required to compensate for the signal transmission when $T_{\text{SW}} \geq 1/2B = 25$ ns. Finally, Fig. 7(g) presents a similar trend for the BER performance of the RF-chain-free system over additive white Gaussian noise channel where the transmitter employs convolution coding with code-rate 1/2, and receiver applies hard-decision Viterbi decoder.

V. Conclusion and Future Direction

In this paper, we presented a framework to design and evaluate agile RF beamformers from theoretical and practical perspectives in wireless systems. In particular, we proposed agile RF beamforming methods for RF-chain-free, analog, and hybrid beamformers considering the impacts of the phase shifters' resolution and speed. To evaluate and compare the system performance, we defined several metrics based on the Gram-Schmidt orthogonalization process. The results indicated that the phase shifters' speed and the number of RF-chains have a more dominant impact on the system performance than the phase shifters' resolution and the number of antennas. The use of slower phase shifters can result in aliasing, in-band distortion, and out-of-band emissions, depending on the signal's bandwidth. To better elaborate on such effects in communication systems, we used extensive simulations to study the impact of switching-time of the phase shifters on the ACLR, achievable sum-rates in different channel models, power efficiency compared to the conventional hybrid beamformers, EVM of 64-QAM constellation and BER. As future directions of this research, it is necessary to further optimize the proposed approaches in order to implement agile RF beamformers in practical systems. For example, the proposed approach for setting the agile hybrid beamforming weights requires the calculation of pseudo-inverse of a matrix for continuous-time signals which imposes significant overhead on the baseband processor. Hence, it is required to explore the time-domain characteristics of the signal, e.g., correlation, to interpolate the beamforming weights, and reduce the number of the matrix inversions. In addition, further optimization of pre/post-processing techniques to reduce the signal distortion, and also a more detailed investigation of the energy efficiency of the proposed approaches, remain as an interesting research directions. Finally, in future, the information-theoretic analysis can be used to characterize the rate-region by agile RF beamformers for more general scenarios.

References

[1] E. G. Larsson, O. Edfors, F. Tufvesson, and T. L. Marzetta, "Massive MIMO for next generation wireless systems," *IEEE Commun. Mag.*, vol. 52, no. 2, pp. 186–195, Feb. 2014.

[2] R. W. Heath, Jr., N. González-Prelcic, S. Rangan, W. Roh, and A. M. Sayeed, "An overview of signal processing techniques for millimeter wave MIMO systems," *IEEE J. Sel. Topics Signal Process.*, vol. 10, no. 3, pp. 436–453, Apr. 2016.

[3] S. Malkowsky *et al.*, "The world's first real-time testbed for massive MIMO: Design, implementation, and validation," *IEEE Access*, vol. 5, pp. 9073–9088, 2017.

[4] B. Yang, Z. Yu, J. Lan, R. Zhang, J. Zhou, and W. Hong, "Digital beamforming-based massive MIMO transceiver for 5G millimeter-wave communications," *IEEE Trans. Microw. Theory Techn.*, vol. 66, no. 7, pp. 3403–3418, Jul. 2018.

[5] Y. Yu, W. Hong, Z. H. Jiang, H. Zhang, and C. Guo, "Multibeam generation and measurement of a DDS-based digital beamforming array transmitter at Ka-band," *IEEE Trans. Antennas Propag.*, vol. 67, no. 5, pp. 3030–3039, May 2019.

[6] S. Zihir, O. D. Gurbuz, A. Kar-Roy, S. Raman, and G. M. Rebeiz, "60-GHz 64-and 256-elements wafer-scale phased-array transmitters using full-reticle and subreticle stitching techniques," *IEEE Trans. Microw. Theory Techn.*, vol. 64, no. 12, pp. 4701–4719, Dec. 2016.

[7] S. Payami *et al.*, "Developing the first mmWave fully-connected hybrid beamformer with a large antenna array," *IEEE Access*, vol. 8, pp. 141282–141291, 2020.

[8] X. Zhang, A. F. Molisch, and S.-Y. Kung, "Variable-phase-shift-based RF-baseband codesign for MIMO antenna selection," *IEEE Trans. Signal Process.*, vol. 53, no. 11, pp. 4091–4103, Nov. 2005.

[9] I. Ahmed *et al.*, "A survey on hybrid beamforming techniques in 5G: Architecture and system model perspectives," *IEEE Commun. Surveys Tuts.*, vol. 20, no. 4, pp. 3060–3097, Jun. 2018.

[10] F. Sohrabi and W. Yu, "Hybrid analog and digital beamforming for mmWave OFDM large-scale antenna arrays," *IEEE J. Sel. Areas Commun.*, vol. 35, no. 7, pp. 1432–1443, Jul. 2017.

[11] S. Payami, M. Ghoraishi, and M. Dianati, "Hybrid beamforming for large antenna arrays with phase shifter selection," *IEEE Trans. Wireless Commun.*, vol. 15, no. 11, pp. 7258–7271, Nov. 2016.

[12] O. E. Ayach, S. Rajagopal, S. Abu-Surra, Z. Pi, and R. W. Heath, Jr., "Spatially sparse precoding in millimeter wave MIMO systems," *IEEE Trans. Wireless Commun.*, vol. 13, no. 3, pp. 1499–1513, Mar. 2014.

[13] X. Gao, L. Dai, S. Han, C.-L. I, and R. W. Heath, Jr., "Energy-efficient hybrid analog and digital precoding for mmWave MIMO systems with large antenna arrays," *IEEE J. Sel. Areas Commun.*, vol. 34, no. 4, pp. 998–1009, Apr. 2016.

[14] Y. Chen, D. Chen, and T. Jiang, "Non-uniform quantization codebook-based hybrid precoding to reduce feedback overhead in millimeter wave MIMO systems," *IEEE Trans. Commun.*, vol. 67, no. 4, pp. 2779–2791, Apr. 2019.

[15] X. Yu, J.-C. Shen, J. Zhang, and K. B. Letaief, "Alternating minimization algorithms for hybrid precoding in millimeter wave MIMO systems," *IEEE J. Sel. Topics Signal Process.*, vol. 10, no. 3, pp. 485–500, Apr. 2016.

[16] Y. Chen, D. Chen, Y. Tian, and T. Jiang, "Spatial lobes division-based low complexity hybrid precoding and diversity combining for mmWave IoT systems," *IEEE Internet Things J.*, vol. 6, no. 2, pp. 3228–3239, Apr. 2019.

[17] Y. Chen, D. Chen, T. Jiang, and L. Hanzo, "Channel-covariance and angle-of-departure aided hybrid precoding for wideband multiuser millimeter wave MIMO systems," *IEEE Trans. Commun.*, vol. 67, no. 12, pp. 8315–8328, Dec. 2019.

[18] A. Arora, C. G. Tsinos, B. S. M. R. Rao, S. Chatzinotas, and B. Ottersten, "Hybrid transceivers design for large-scale antenna arrays using majorization-minimization algorithms," *IEEE Trans. Signal Process.*, vol. 68, pp. 701–714, Dec. 2020.

[19] M. A. Sedaghat, V. I. Barousis, R. R. Müller, and C. B. Papadias, "Load modulated arrays: A low-complexity antenna," *IEEE Commun. Mag.*, vol. 54, no. 3, pp. 46–52, Mar. 2016.

[20] B. Gäde, M. Amon, A. Bereyhi, G. Fischer, and R. R. Müller, "Outphasing elements for hybrid analogue digital beamforming and single-RF MIMO," in *Proc. IEEE Int. Conf. Acoust., Speech Signal Process. (ICASSP)*, May 2019, pp. 7839–7843.

[21] A. Morsali, A. Haghighat, and B. Champagne, "Realizing fully digital precoders in hybrid A/D architecture with minimum number of RF chains," *IEEE Commun. Lett.*, vol. 21, no. 10, pp. 2310–2313, Oct. 2017.

[22] A. Morsali, S. Norouzi, and B. Champagne, "Single RF chain hybrid analog/digital beamforming for mmWave massive-MIMO," in *Proc. Global Conf. Signal Inf. Process. (GlobalSIP)*, Nov. 2019, pp. 1–5.

[23] A. Morsali and B. Champagne, "Achieving fully-digital performance by hybrid analog/digital beamforming in wide-band massive-MIMO systems," in *Proc. IEEE Int. Conf. Acoust., Speech Signal Process. (ICASSP)*, May 2020, pp. 5125–5129.

[24] C. G. Tsinos, S. Maleki, S. Chatzinotas, and B. Ottersten, "On the energy-efficiency of hybrid analog–digital transceivers for single-and multi-carrier large antenna array systems," *IEEE J. Sel. Areas Commun.*, vol. 35, no. 9, pp. 1980–1995, Sep. 2017.
[25] J. G. Proakis and D. K. Manolakis, *Digital Signal Processing*, 4th ed. Upper Saddle River, NJ, USA: Prentice-Hall, 2006.
[26] J. Volakis, R. Johnson, and H. Jasik, *Antenna Engineering Handbook*, 4th ed. New York, NY, USA: McGraw-Hill, 2007.
[27] *MATLAB Version 9.9.0.1467703 (R2020b)*, Mathworks, Natick, MA, USA, 2020.
[28] *Base Station (BS) Conformance Testing Part 1: Conducted Conformance Testing (Release 16)*, document TS 38.141-1, 3GPP Technical Specification Group Radio Access Network, Sep. 2020.
[29] *Study on New Radio Access Technology: Radio Frequency (RF) and Co-Existence Aspects (Release 14)*, document TR 38.803, Sep. 2017.
[30] S. Payami, M. Khalily, S. Taheri, K. Nikitopoulos, and R. Tafazolli, "Channel measurement and analysis for polarimetric wideband outdoor scenarios at 26 GHz: Directional vs omni-directional," in *Proc. 14th Eur. Conf. Antennas Propag. (EuCAP)*, Mar. 2020, pp. 1–5.
[31] A. Alkhateeb and R. W. Heath, Jr., "Frequency selective hybrid precoding for limited feedback millimeter wave systems," *IEEE Trans. Commun.*, vol. 64, no. 5, pp. 1801–1818, May 2016.
[32] A. Li and C. Masouros, "Hybrid precoding and combining design for millimeter-wave multi-user MIMO based on SVD," in *Proc. IEEE Int. Conf. Commun. (ICC)*, May 2017, pp. 1–6.
[33] R. Méndez-Rial, C. Rusu, N. González-Prelcic, A. Alkhateeb, and R. W. Heath, Jr., "Hybrid MIMO architectures for millimeter wave communications: Phase shifters or switches?" *IEEE Access*, vol. 4, pp. 247–267, 2016.

Sohail Payami (Member, IEEE) received the M.Sc. degree from Lund University and the Ph.D. degree from the University of Surrey. He has worked as a Research Assistant with Lund University and an Intern with the Imperial College of London. He was a Research Associate with Heriot–Watt University. He is currently a Research Fellow with the Institute for Communication Systems, University of Surrey. His research interests include signal processing for massive MIMO and mmWave systems.

Konstantinos Nikitopoulos (Senior Member, IEEE) is currently a Reader of Signal Processing for Communication Systems with the Electrical and Electronic Engineering Department, Institute for Communication Systems, University of Surrey, Guildford, U.K. He is also a member of the 5G and 6G Innovation Centres, where he leads the "Theory and Practice of Advanced Concepts in Wireless Communications" work area, and the Director of the Wireless Systems Laboratory, Institute for Communication Systems. He has held research positions with RWTH Aachen University, Germany, the University of California at Irvine, Irvine, CA, USA, and University College London, U.K. He was a recipient of the prestigious First Grant of the UK's Engineering and Physical Sciences Research Council, and the Principal Investigator of several research projects, including AutoAir I and II projects, UK's 5G Testbeds, and Trials Programme.

Mohsen Khalily (Senior Member, IEEE) is currently a Lecturer in antenna and propagation with the Home of the 5G and 6G Innovation Centres (5GIC and 6GIC), Institute for Communication Systems (ICS), University of Surrey, U.K., where he was a Research Fellow on antennas and propagation from December 2015 to March 2019. Prior to joining the 5GIC, he was a Senior Lecturer with the Wireless Communication Centre (WCC), University Technology Malaysia (UTM). He has published almost 120 academic papers in international peer-reviewed journals and conference proceedings. His research interests include surface electromagnetic, reconfigurable reflecting surface, 5G systems, phased arrays, hybrid beamforming, and mm-wave and terahertz antennas and propagation. He is also a member of the IEEE Antennas and Propagation Society, the IEEE Communication Society, and the IEEE Microwave Theory and Techniques Society. He is a fellow of the U.K. Higher Education Academy. He is an Associate Editor of IEEE ACCESS.

Rahim Tafazolli (Senior Member, IEEE) is a Regius Professor of Electronic Engineering, a fellow of the Royal Academy of Engineering, (FREng), FIET, and WWRF, a Professor of Mobile and Satellite Communications, and the Founder and the Director of 5GIC, 6GIC and ICS (Institute for Communication System) with the University of Surrey. He has over 30 years of experience in digital communications research and teaching. He has authored and coauthored more than 1000 research publications. He is regularly invited to deliver keynote talks and distinguished lectures to international conferences and workshops, and also invited by many governments for advice on 5G technologies. He was an Advisor to the Mayor of London in regard to the London Infrastructure Investment 2050 Plan. He has given many interviews to international media in the form of television, radio interviews, and articles in international press.